



TECHNISCHE
UNIVERSITÄT
MÜNCHEN

Spherical harmonic computations with topographic/isostatic coefficients

D. Tsoulis

IAPG / FESG No. 3

Institut für Astronomische und Physikalische Geodäsie
Forschungseinrichtung Satellitengeodäsie

München 1999

Spherical harmonic computations with topographic/isostatic coefficients

Dimitrios Tsoulis

Institut für Astronomical and Physical Geodesy (IAPG), Technische Universität München
D-80290 München, Germany (email: tsoulis@step.iapg.verm.tu-muenchen.de)

Abstract

This report comprises two parts. In the first part different methods of spherical harmonic analysis on the sphere are presented with emphasis on the loss of orthogonality in the direction of latitude due to the transition from the continuous to the discretized case. The difference between the use of mean and point values is stressed and a part of the study is dedicated to the recursive computation of the integrals of the associated Legendre functions. The computation of topographic/isostatic potential harmonic coefficients from a global elevation model accounting for the compensation of the topography according to a standard isostatic model is presented in detail in the second part of the present report. The theory is based on a series expansion of the inverse distance function which enables an efficient computation on the sphere of the dimensionless potential coefficients \overline{C}_{lm} and \overline{S}_{lm} . In this derivation the isostatic compensation of the Earth's topography is taken into account. The idealized isostatic models of Airy/Heiskanen and Pratt/Hayford are considered. From the potential coefficients related functionals of the gravitational field can be easily derived by applying a global spherical harmonic synthesis taking into consideration the appropriate eigenvalues according to the standard Meissl scheme. This has been applied for the region surrounding the European Alps. The possibility of implementing a spherical harmonic synthesis in a regional scale offers the advantage of observing and interpreting regional characteristics of the gravity field as well as investigating the suitability of the used isostatic model for the specific region.

1 Introduction

Global spherical harmonic analysis (GSHA) is a term used to describe the reduction of global data sets to spherical harmonic coefficients. Mathematically this is analogous to an inverse 2-D Fourier transform: the coefficients \overline{C}_{lm} and \overline{S}_{lm} are estimated from the known signal given on a sphere. The forward computation, which is the computation of a function on a sphere from a series of surface spherical harmonics, is known as global spherical harmonic synthesis (GSHS). The pair of GSHS and GSHA build the system of global spherical harmonic computation (GSHC). The numerical algorithms, both for synthesis and for analysis, can be based on a two-step formulation in the continuous as well in the discrete case by separating the computation in the direction of longitude from the one in the direction of latitude. Although the former can be performed easily for discrete as well as continuous data, the integration in the direction of latitude exhibits difficulties arising from the loss of orthogonality of Legendre functions at discrete points. Different approaches have been used in the literature to overcome this problem. Gauss's least squares, approximate quadrature and weighted least-squares solutions, known as Neumann's exact methods, are the most common ones. Sneeuw (1994) gives an overview of these methods and recasts the discrete analysis and synthesis formulae into matrix-vector equations. Error considerations for the GSHC formulae can be found in Colombo (1981).

We consider at first the standard GSHC matrix-vector formulation, as given by Sneeuw (1994), emphasizing on the loss of orthogonality of the Legendre functions when one makes the transition from the continuous into the discrete case. The need for the use of the integrals of the associated Legendre functions when using so called "area means" is stressed and the iterative computation of the

associated Legendre functions as well as their integrals is presented in detail. Then we concentrate on the harmonic analysis of a global elevation model, applying the theory laid out in the previous sections. In doing this the isostatic compensation of the Earth's topography is taken into account according to established theory presented by Sünkel (1986), Rummel et al. (1988) and others. Both idealized isostatic models of Airy/Heiskanen and Pratt/Hayford are considered. From the obtained potential harmonic coefficients a connection to other related functionals of the gravitational field can be directly established by means of the known eigenvalues relating the gravity disturbance potential, its first and its second radial derivative according to the so-called Meissl scheme (Rummel 1991; Rummel and van Gelderen 1995). We conclude with a spherical harmonic synthesis application of a global set of topographic/isostatic derived spherical harmonic coefficients in a regional scale. The structure of the involved matrices in the matrix-vector formulation of the GSHS algorithm enables such a computation. The area surrounding the European Alps has been selected for these computations ($40^\circ \leq \vartheta \leq 50^\circ$; $0^\circ \leq \lambda \leq 20^\circ$). The adequacy of the isostatic models used, can be observed easily in this example. Furthermore, a regional spherical harmonic synthesis offers a better insight into the local characteristics of the observed gravity field.

A Review of Spherical Harmonic Analysis and Synthesis

2 Global spherical harmonic analysis and synthesis with point data

A square integrable, analytical function $f(\theta, \lambda)$ defined on the unit sphere (θ co-latitude, λ longitude) can be expanded in a series of spherical harmonics (Colombo, 1981)

$$f(\theta, \lambda) = \sum_{l=0}^{\infty} \sum_{m=0}^l \bar{P}_{lm}(\cos \theta) \left(\bar{C}_{lm} \cos m\lambda + \bar{S}_{lm} \sin m\lambda \right) \quad (1)$$

where l , m denote degree and order respectively, \bar{P}_{lm} are the fully normalized associated Legendre functions and \bar{C}_{lm} , \bar{S}_{lm} are the fully normalized spherical harmonic coefficients. The normalization factor used is (Heiskanen and Moritz 1967, eq. (1-73))

$$N_{lm} = \sqrt{(2 - \delta_{m0})(2l + 1) \frac{(l - m)!}{(l + m)!}} \quad ,$$

with

$$\delta_{m0} = \begin{cases} 1, & m = 0, \\ 0, & m \neq 0. \end{cases}$$

It can be shown (Colombo, 1981) that a surface spherical harmonic series such as (1) where the highest degree is L_{max} is identical to a 2-D Fourier series, where the highest l and m are also L_{max} , in the domain $-\pi \leq \theta \leq \pi$, $0 \leq \lambda \leq 2\pi$. The converse is not true, because continuous functions on a sphere, such as $\bar{P}_{lm}(\cos \theta) \sin m\lambda$ and $\bar{P}_{lm}(\cos \theta) \cos m\lambda$ appearing in (1), must satisfy certain conditions at the poles. Spherical harmonics correspond to a subclass of 2-D Fourier series.

Inverting equation (1) one obtains the GSHA system of equations

$$\left. \begin{matrix} \bar{C}_{lm} \\ \bar{S}_{lm} \end{matrix} \right\} = \frac{1}{4\pi} \iint_{\sigma} f(\theta, \lambda) \bar{P}_{lm}(\cos \theta) \begin{Bmatrix} \cos m\lambda \\ \sin m\lambda \end{Bmatrix} d\sigma \quad , \quad (2)$$

with $d\sigma = \sin\theta d\theta d\lambda$. Both, equations (1) and (2) represent the continuous case of the global spherical harmonic computation equations and they can be rewritten in a two-step formulation where the latitude and longitude information are dealt with independently. This enables efficient computer programming and application of Fourier transformations over individual parallels. In the sequel the discrete form of equations (1) – (2) using the two-step formulation will be presented. At the same time we concentrate on the transition from the analytical to the discrete case.

In practice one has to deal with information at discrete points or block averages . Thus, equation (1) is truncated at a specific degree L , and (2) cannot be calculated analytically: it is replaced by a summation corresponding to the discrete data $f(\theta, \lambda)$ given on the sphere. The discrete form of equation (1) in a two-step formulation given an equi-angular discretization in λ -direction $\lambda_k = k\Delta\lambda$, $k = 0, 1, \dots, 2L - 1$, where

$$\Delta\lambda = \frac{2\pi}{2L} = \frac{\pi}{L} ,$$

is the following set of equations

$$\left. \begin{array}{l} A_m(\theta_i) \\ B_m(\theta_i) \end{array} \right\} = \sum_{l=m}^L \bar{P}_{lm}(\cos\theta_i) \left\{ \begin{array}{l} \bar{C}_{lm} \\ \bar{S}_{lm} \end{array} \right. , \quad (3a)$$

$$f(\theta_i, \lambda_k) = \sum_{m=0}^L A_m(\theta_i) \cos m\lambda_k + B_m(\theta_i) \sin m\lambda_k . \quad (3b)$$

The subscripts i and k are used to designate the position of the sample in the two-dimensional array: i corresponds always to latitude and k to longitude. The two-step formulation for the analysis equation (2) is more complicated. While with the discretization in the longitude direction orthogonality is preserved (see e.g. Sneeuw 1994, section 2.2), the latitude sampling must be treated explicitly due to the fact that discretization in the direction of latitude destroys the orthogonality of the Legendre functions. At this point it is important to distinguish between the two possibilities in creating a grid of point data. The data grid should be conceived as a two-dimensional array containing the samples of $f(\theta, \lambda)$ covering in some more or less regular way the sphere. In the ideal case the data corresponds to a set of complete parallels and meridians. However in reality some cells in this grid may be empty due to lack of information, as for example in the polar regions. When one deals with *point data* the area of these cells are taken into account when the data is derived averaging the information being inside each cell. In the implementation of the analysis equation however the area of the cells is absent from the computations. There are two ways of defining such a grid: when the point data consist of values of $f(\theta, \lambda)$ determined at the intersections of the grid, they are referred to as *intersections*; if they refer to the centers of the blocks defined by the lines of the grid, then they are called *block centers*. Assuming an equi-angular discretization in longitudinal direction as already defined above, it can be shown that orthogonality is preserved in the λ -direction both for intersections and block centers (Sneeuw 1994; Albertella and Sacerdote 1995). For intersections the following relations hold

$$\sum_{k=0}^{2L-1} \cos m\lambda_k \cos n\lambda_k = (1 + \delta_{m0} + \delta_{mL}) L\delta_{mn} , \quad \lambda_k = k\Delta\lambda, \quad k = 0, 1, \dots, 2L - 1 ,$$

$$\sum_{k=0}^{2L-1} \sin m\lambda_k \sin n\lambda_k = (1 - \delta_{m0} - \delta_{mL}) L\delta_{mn} , \quad \lambda_k = k\Delta\lambda, \quad k = 0, 1, \dots, 2L - 1 ,$$

$$\sum_{k=0}^{2L-1} \cos m\lambda_k \sin n\lambda_k = 0 , \quad \lambda_k = k\Delta\lambda, \quad k = 0, 1, \dots, 2L - 1 .$$

For block centers, i.e. for sample points taken at the centers of equi-angular blocks, (θ_i, λ_k) , $\theta_i = i\Delta\theta$, $i = 1, 2, \dots, L$, $\lambda_k = k\Delta\lambda$, $k = 1, 2, \dots, 2L$ and $\Delta\theta = \Delta\lambda = \pi/L$, the discrete orthogonality in the longitudinal direction is expressed by

$$\begin{aligned} \sum_{k=1}^{2L} \cos m\lambda_k \cos n\lambda_k &= (1 + \delta_{m0} - \delta_{mL}) L\delta_{mn} \quad , \quad \lambda_k = \frac{\Delta\lambda}{2} + k\Delta\lambda, \quad k = 0, 1, \dots, 2L - 1 \quad , \\ \sum_{k=1}^{2L} \sin m\lambda_k \sin n\lambda_k &= (1 - \delta_{m0} + \delta_{mL}) L\delta_{mn} \quad , \quad \lambda_k = \frac{\Delta\lambda}{2} + k\Delta\lambda, \quad k = 0, 1, \dots, 2L - 1 \quad , \\ \sum_{k=1}^{2L} \cos m\lambda_k \sin n\lambda_k &= 0 \quad , \quad \lambda_k = \frac{\Delta\lambda}{2} + k\Delta\lambda, \quad k = 0, 1, \dots, 2L - 1 \quad . \end{aligned}$$

The above triads of equations express the preservation of orthogonality in the discrete case for the longitudinal direction for intersections and block centers respectively. For both grids of point data the orthogonality in the direction of latitude is lost, in other words it is

$$\sum_{i=1}^N \bar{P}_{l_1 m}(\cos \theta_i) \bar{P}_{l_2 m}(\cos \theta_i) \neq 2(2 - \delta_{m0}) \delta_{l_1 l_2} \quad ,$$

where N denotes the number of parallels, not necessarily equal to L . The first step of the discrete case of GSHA for point data will be given by the following linear system of equations

$$\left. \begin{array}{l} A_m(\theta_i) \\ B_m(\theta_i) \end{array} \right\} = \left\{ \begin{array}{l} \frac{1}{L(1 + \delta_{m0} + \delta_{mL})} \\ \frac{1}{L(1 - \delta_{m0} - \delta_{mL})} \end{array} \right\} \sum_{k=0}^{2L-1} f(\theta_i, \lambda_k) \left\{ \begin{array}{l} \cos m\lambda_k \\ \sin m\lambda_k \end{array} \right. \quad . \quad (4a)$$

In the case of block centers one obtains respectively

$$\left. \begin{array}{l} A_m(\theta_i) \\ B_m(\theta_i) \end{array} \right\} = \left\{ \begin{array}{l} \frac{1}{L(1 + \delta_{m0} - \delta_{mL})} \\ \frac{1}{L(1 - \delta_{m0} + \delta_{mL})} \end{array} \right\} \sum_{k=0}^{2L-1} f(\theta_i, \lambda_k) \left\{ \begin{array}{l} \cos m\lambda_k \\ \sin m\lambda_k \end{array} \right. \quad . \quad (4b)$$

The θ -sampling choice leads to the respective discrete solution in the second step of spherical harmonic analysis. One can categorize these solutions into approximate and exact ones. The former ignore non-orthogonality or assign to each parallel θ_i a quadrature weight independent from degree and order. In the latter exact orthogonality can be produced by devising the weights in such a way that they fulfill certain conditions; these solutions are known from the work of Neumann and are referred to as Neumann's methods. Before reviewing the different solutions let us rewrite the discrete analysis and synthesis formulae using matrix-vector notation. We introduce the vectors $\mathbf{a} = [A_m(\theta_1) \ A_m(\theta_2) \ \dots \ A_m(\theta_N)]^\top$, $\mathbf{b} = [B_m(\theta_1) \ B_m(\theta_2) \ \dots \ B_m(\theta_N)]^\top$, $\mathbf{c} = [\bar{C}_{mm} \ \bar{C}_{m+1,m} \ \dots \ \bar{C}_{Lm}]^\top$, $\mathbf{s} = [\bar{S}_{mm} \ \bar{S}_{m+1,m} \ \dots \ \bar{S}_{Lm}]^\top$ and $\mathbf{f} = [f(\theta_i, \lambda_0) \ f(\theta_i, \lambda_1) \ \dots \ f(\theta_i, \lambda_{2L-1})]^\top$. The length of \mathbf{a} and \mathbf{b} is N , \mathbf{c} and \mathbf{s} are both of dimensions $(L - m + 1) \times 1$, while \mathbf{f} has $2L$ elements. Furthermore a $N \times (L - m + 1)$ matrix \mathbf{P} for the fully normalized Legendre functions can be defined as

$$\mathbf{P} = \begin{bmatrix} \overline{P}_{mm}(\cos \theta_1) & \overline{P}_{m+1,m}(\cos \theta_1) & \cdots & \overline{P}_{Lm}(\cos \theta_1) \\ \overline{P}_{mm}(\cos \theta_2) & \ddots & & \vdots \\ \vdots & & \ddots & \vdots \\ \overline{P}_{mm}(\cos \theta_N) & \cdots & \cdots & \overline{P}_{Lm}(\cos \theta_N) \end{bmatrix}.$$

Finally for the recasting of equation (1) into a matrix-vector notation we introduce the $2L \times 2L$ Fourier matrix \mathbf{F} with entries (Strang 1986)

$$[\mathbf{F}]_{rs} = e^{j(rs\pi)/L} = \cos \frac{rs\pi}{L} + j \sin \frac{rs\pi}{L}, \quad r, s = 0, 1, \dots, 2L - 1$$

and a complex vector \mathbf{d} of length $2L$ composed of $\mathbf{a} + j\mathbf{b}$ and $\mathbf{a} - j\mathbf{b}$, with j being the imaginary unit ($j^2 = -1$). Now the discrete formulae for the global spherical harmonic synthesis can be written as follows:

$$\mathbf{a} = \mathbf{P}\mathbf{c}, \quad \mathbf{b} = \mathbf{P}\mathbf{s} \quad (5a)$$

and

$$\mathbf{f} = \mathbf{F}\mathbf{d} \quad (5b)$$

Equations (5a) and (5b) correspond to (3a) and (3b) and are best suited for numerical implementation with a computer. Solving equation (5b) for \mathbf{d} one obtains directly

$$\mathbf{d} = \mathbf{F}^{-1}\mathbf{f}. \quad (6a)$$

From this vector one can derive \mathbf{a} and \mathbf{b} and thus the first step of GSHA is completed. As mentioned earlier there are different approaches for solving the second analysis step, depending on the way the θ -sampling problem is solved. A first type of approximation arises when a least-squares solution of the linear systems (5a) is applied:

$$\mathbf{c} = (\mathbf{P}^\top \mathbf{P})^{-1} \mathbf{P}^\top \mathbf{a}, \quad \mathbf{s} = (\mathbf{P}^\top \mathbf{P})^{-1} \mathbf{P}^\top \mathbf{b}. \quad (7)$$

It will be referred to as the least squares (LS) method. As an alternative, one can introduce to each parallel θ_i a corresponding weight s_i , proportional to the sine of the colatitude:

$$s_i = \frac{2}{\sum_{n=1}^N \sin \theta_n} \sin \theta_n.$$

Denoting with \mathbf{S} the diagonal weight matrix, whose diagonal consists of the s_i weights, one obtains a weighted least squares solution (WLS) of the second spherical harmonic analysis step

$$\mathbf{c} = (\mathbf{P}^\top \mathbf{S} \mathbf{P})^{-1} \mathbf{P}^\top \mathbf{S} \mathbf{a}, \quad \mathbf{s} = (\mathbf{P}^\top \mathbf{S} \mathbf{P})^{-1} \mathbf{P}^\top \mathbf{S} \mathbf{b}. \quad (8)$$

To a good extent the normal matrix of this least squares solution equals a scaled identity matrix, i.e. it holds $\mathbf{P}^\top \mathbf{S} \mathbf{P} \approx 2(2 - \delta_{m0}) \mathbf{I}$. Thus, from equation (8) an additional method emerges, namely the approximate quadrature method (AQ)

$$\mathbf{c} = \frac{1}{4} (1 + \delta_{m0}) \mathbf{P}^\top \mathbf{S} \mathbf{a}, \quad \mathbf{s} = \frac{1}{4} (1 + \delta_{m0}) \mathbf{P}^\top \mathbf{S} \mathbf{b}. \quad (9)$$

So far the non-orthogonality of the Legendre functions in the θ -direction has been ignored. The exact methods of Neumann guarantee discrete orthogonality by defining the weights assigned to each parallel θ_i in such a way that they fulfill the following condition

$$\sum_{i=1}^N w_i \cos^n \theta_i = \begin{cases} \frac{2}{n+1}, & n \text{ even,} \\ 0, & n \text{ odd,} \end{cases}$$

with $n = 0, 1, \dots, N-1$ and N the total number of parallels. It can be shown, (Sneeuw 1994), that with this definition of the latitude weights w_i the orthogonality of the Legendre functions in θ -direction is retrieved. If the w_i are stored in a diagonal weight matrix \mathbf{W} , the exact solution to the second analysis step or equally Neumann's exact method will be given by the following weighted least squares solution

$$\begin{aligned} \mathbf{c} &= (\mathbf{P}^\top \mathbf{W} \mathbf{P})^{-1} \mathbf{P}^\top \mathbf{W} \mathbf{a} \equiv \frac{1}{4} (1 + \delta_{m0}) \mathbf{P}^\top \mathbf{W} \mathbf{a}, \\ \mathbf{s} &= (\mathbf{P}^\top \mathbf{W} \mathbf{P})^{-1} \mathbf{P}^\top \mathbf{W} \mathbf{b} \equiv \frac{1}{4} (1 + \delta_{m0}) \mathbf{P}^\top \mathbf{W} \mathbf{b}. \end{aligned} \tag{10}$$

Although the weights given to each parallel are defined above, the θ -sampling has not been settled yet. In principle, there are two possibilities of defining the θ -spacing, each of which leads to a different version of the exact Neumann method. In the so-called first Neumann method (FNM) the parallels are chosen randomly but are distinct, i.e. we do not have coinciding parallels; one such choice could be an equi-angular $\Delta\theta$ spacing. The second case of exact quadrature (Second Neumann Method; SNM) is achieved by restricting the θ -grid to the one used in *Gaussian quadrature* (Krylov 1962). Here the latitude circles are chosen so that they coincide with the zeros of the Legendre polynomials of degree $L+1$, i.e. those θ_i 's for which $P_{L+1}(\cos \theta_i) = 0$, $i = 1, 2, \dots, L+1$.

Table 1 shows that all methods except for the second Neumann method, can be applied using either an equi-angular or a Gaussian θ -grid. The SNM, however, is exclusively employable on a Gaussian grid.

Table 1. Different θ grids for point data with respect to the method used in the second step in GSHA. Thereby λ is assumed to be sampled on an equi-angular grid. The signs $+/-$ denote respectively compatibility or not of grid with method.

| Method | θ -grid | |
|--------|----------------|----------|
| | equi-angular | Gaussian |
| LS | + | + |
| WLS | + | + |
| AQ | + | + |
| FNM | + | + |
| SNM | - | + |

3 Global spherical harmonic analysis with block means

Up to now only point data were considered. It is possible however that data, for the case of a global elevation model the elevation values, refer to mean values corresponding to the blocks defined by the

meridians and parallels of the data-grid. The proper use of such *block means* requires a modification of the formulas presented in the previous section. In particular, it incorporates into the algorithm the computation of the integrals of the fully normalized associated Legendre functions. The use of block means actually suggests that the area of the respective block has somehow to be taken into account. The point information is now replaced with an integration along the parallels in the first step of the discrete GSHA and an integration along the meridians in the computation of \overline{C}_{lm} and \overline{S}_{lm} in the second step. In the latter step, the integrals of the associated Legendre functions enter the algorithm. Recursive relations for their computation are available from the literature and are presented in the following section. We present now in detail the two steps of the discrete GSHA with block means. The first step of the GSHA formulation was given for point values by equation (4b). This equation should be properly written for block means as follows

$$\left. \begin{array}{l} \overline{A}_m(\theta_i) \\ \overline{B}_m(\theta_i) \end{array} \right\} = \left\{ \begin{array}{l} \frac{1}{L(1 + \delta_{m0} - \delta_{mL})} \\ \frac{1}{L(1 - \delta_{m0} + \delta_{mL})} \end{array} \right\} \sum_{k=0}^{2L-1} f(\theta_i, \lambda_k) \left\{ \begin{array}{l} \int_{\lambda_{k-1}}^{\lambda_k} \cos m\lambda \, d\lambda \\ \int_{\lambda_{k-1}}^{\lambda_k} \sin m\lambda \, d\lambda \end{array} \right. . \quad (11)$$

The integrals along the longitude direction have closed analytical solutions, namely

$$\text{IC}_m(\lambda_k) = \int_{\lambda_1}^{\lambda_2} \cos m\lambda \, d\lambda = \frac{2}{m} \cos m \frac{\lambda_2 + \lambda_1}{2} \sin m \frac{\Delta\lambda}{2} \quad (12)$$

and

$$\text{IS}_m(\lambda_k) = \int_{\lambda_1}^{\lambda_2} \sin m\lambda \, d\lambda = \frac{2}{m} \sin m \frac{\lambda_2 + \lambda_1}{2} \sin m \frac{\Delta\lambda}{2} , \quad (13)$$

where $\Delta\lambda = \lambda_{k+1} - \lambda_k$, or for the case of an equi-angular sampling $\Delta\lambda = \pi/L$. To observe better the transition from point to block means in the second step of spherical harmonic analysis it would be useful to write the continuous case of the second step of GSHA (Sneeuw 1994; eq. (3d))

$$\left. \begin{array}{l} \overline{C}_{lm} \\ \overline{S}_{lm} \end{array} \right\} = \frac{1 + \delta_{m0}}{4} \int_0^\pi \left\{ \begin{array}{l} A_m(\theta) \\ B_m(\theta) \end{array} \right\} \overline{P}_{lm}(\cos \theta) \sin \theta \, d\theta . \quad (14)$$

Rewriting equation (14) for block means yields

$$\left. \begin{array}{l} \overline{C}_{lm} \\ \overline{S}_{lm} \end{array} \right\} = \frac{1 + \delta_{m0}}{4} \sum_{i=1}^N \left\{ \begin{array}{l} \overline{A}_m(\theta_i) \\ \overline{B}_m(\theta_i) \end{array} \right\} \int_{\theta_{i-1}}^{\theta_i} \overline{P}_{lm}(\cos \theta) \sin \theta \, d\theta , \quad (15)$$

with $\overline{A}_m(\theta_i)$ and $\overline{B}_m(\theta_i)$ given by equation (11). The next section is devoted to the computation of the integrals of the associated Legendre functions involved in (15).

4 Fully normalized associated Legendre functions and their integrals

The computation of the fully normalized associated Legendre functions \overline{P}_{lm} appearing in the GSHC discrete formulation for point data is based on the following recurrence relations (Lense 1954; Hobson 1955; Heiskanen & Moritz 1967):

$$\overline{P}_{ll}(\cos \theta) = W_{ll} \sin \theta \overline{P}_{l-1,l-1}(\cos \theta) \quad (16)$$

$$\overline{P}_{l,l-1}(\cos \theta) = W_{ll} \cos \theta \overline{P}_{l-1,l-1}(\cos \theta) \quad (17)$$

$$\overline{P}_{lm}(\cos \theta) = W_{lm} \left[\cos \theta \overline{P}_{l-1,m}(\cos \theta) - W_{l-1,m}^{-1} \overline{P}_{l-2,m}(\cos \theta) \right] , \quad (18)$$

where $m = 0, 1, 2, \dots$ and $l \geq m$,

$$W_{1,1} = \sqrt{3} , \quad (19)$$

$$W_{l,l} = \sqrt{\frac{2l+1}{2l}} \quad \text{with } l > 1 \quad \text{and} \quad (20)$$

$$W_{l,m} = \sqrt{\frac{(2l+1)(2l-1)}{(l+m)(l-m)}} . \quad (21)$$

For the initialization of equations (16), (17) and (18) it holds, respectively, $\overline{P}_{00} = 1$ and $\overline{P}_{m-1,m} = 0$. From these relations one can derive an entirely recursive procedure for the calculation of the set of integrals

$$\overline{\mathbb{P}}_{lm} = \int_{\theta_1}^{\theta_2} \overline{P}_{lm}(\cos \theta) \sin \theta d\theta \quad , \quad m \geq 0 , \quad l \geq m , \quad (22)$$

already referred to as integrals of the associated Legendre functions. They appear in equation (15). Departing from equations (16) – (20) one arrives at the following recurrence relations (Paul 1978; Gerstl 1980):

$$\begin{aligned} \overline{\mathbb{P}}_{ll} = & \frac{W_{ll}}{l+1} \left\{ l W_{l-1,l-1} \overline{\mathbb{P}}_{l-2,l-2} - \cos \theta_2 W_{ll}^{-1} \overline{P}_{ll}(\cos \theta_2) \right. \\ & \left. + \cos \theta_1 W_{ll}^{-1} \overline{P}_{ll}(\cos \theta_1) \right\} , \end{aligned} \quad (23)$$

$$\overline{\mathbb{P}}_{l,l-1} = \frac{W_{lm}}{m+1} \left\{ \sin^2 \theta_2 \overline{P}_{l-1,m}(\cos \theta_2) - \sin^2 \theta_1 \overline{P}_{l-1,m}(\cos \theta_1) \right\} \quad (24)$$

$$\begin{aligned} \overline{\mathbb{P}}_{lm} = & \frac{W_{lm}}{m+1} \left\{ (l-2) W_{l-1,m}^{-1} \overline{\mathbb{P}}_{l-2,m} + \sin^2 \theta_2 \overline{P}_{l-1,m}(\cos \theta_2) \right. \\ & \left. - \sin^2 \theta_1 \overline{P}_{l-1,m}(\cos \theta_1) \right\} . \end{aligned} \quad (25)$$

The recurrence relations (23) – (25) start with the initial values

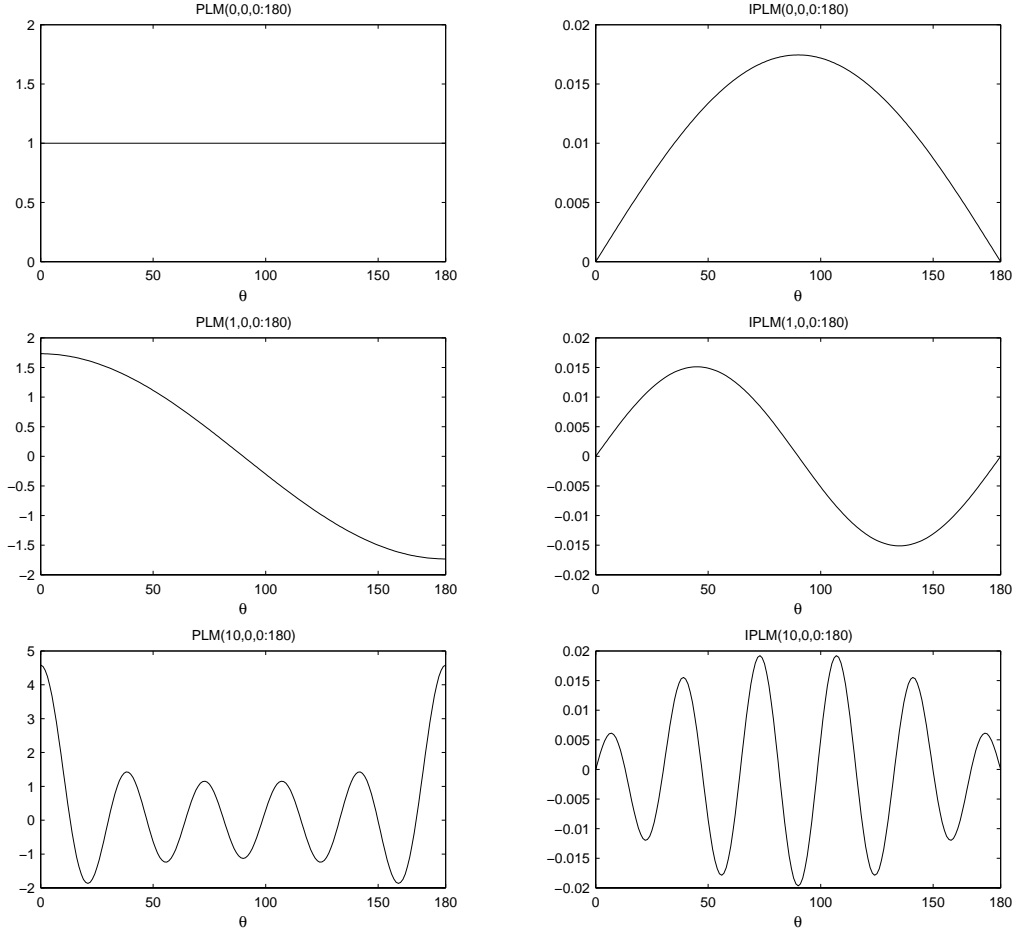


Figure 1: A few examples for \overline{P}_{lm} and \overline{IP}_{lm} for $\theta = 0, \pi/180, 2\pi/180, \dots, \pi$.

$$\overline{IP}_{00} = \cos \theta_1 - \cos \theta_2 , \quad (26)$$

$$\begin{aligned} \overline{IP}_{11} &= W_{11} \frac{1}{2} \left\{ \theta_2 - \theta_1 - \cos \theta \sin \theta \left| \begin{array}{l} \theta_1 \\ \theta_2 \end{array} \right. \right\} \\ &= W_{11} \frac{1}{2} \{ \theta_2 - \theta_1 - \cos \theta_2 \sin \theta_2 + \cos \theta_1 \sin \theta_1 \} \end{aligned} \quad (27)$$

and

$$\overline{IP}_{m-1,m} = 0 . \quad (28)$$

Fig. 1 and Fig. 2 display some fully normalized associated Legendre functions and their respective integrals for an equi-angular θ -sampling, i.e. $\theta = 0, \pi/180, 2\pi/180, \dots, \pi$. One observes that the \overline{IP}_{lm} are symmetric functions with respect to the equator, exactly like the \overline{P}_{lm} but they fluctuate numerically in a scale which is two orders of magnitude smaller than that of \overline{P}_{lm} . This fact is demonstrated by Fig. 3 where both \overline{P}_{lm} and \overline{IP}_{lm} for $l = 13$ and $m = 4$ are drawn in a single

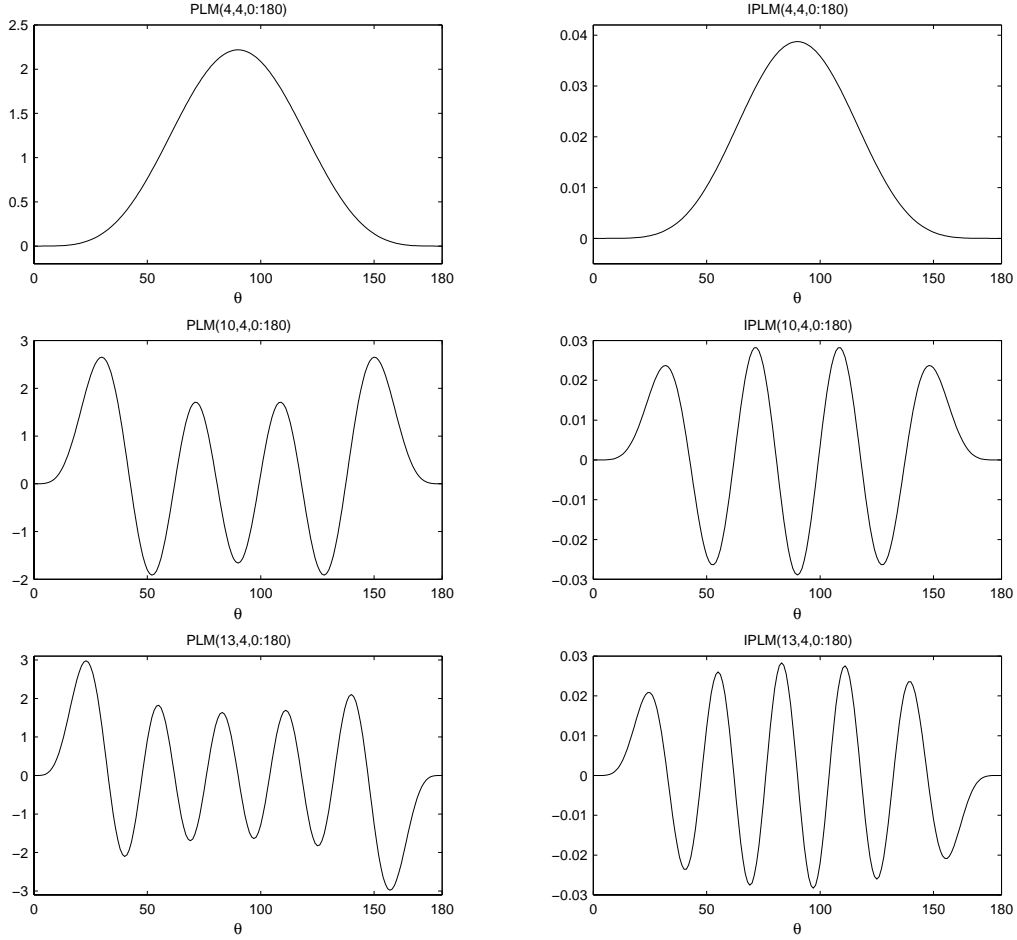


Figure 2: A few examples for \overline{P}_{lm} and \overline{IP}_{lm} for $\theta = 0, \pi/180, 2\pi/180, \dots, \pi$.

graph. It is worth mentioning that the validity of the \overline{IP}_{lm} 's numerical values was proved by means of a numerical evaluation of the integrals (22) with MATLAB's function `quad8` which performs a numerical integration within a relative error of $1e-3$ using an adaptive recursive Newton Cotes 8 panel rule. The agreement between the recursive computation of the \overline{IP}_{lm} according to equations (23) – (27) and a numerical computation using `quad8` reaches the internal accuracy level of the MATLAB numerical package: the difference between the two methods in the computation of $\overline{IP}_{13,4}$ for $\theta = 0, \pi/180, 2\pi/180, \dots, \pi$ has a mean value of $1.8E-16$. We conclude the comparison between the two functions with Fig. 4. Displayed is here the recursion scheme for the computation of $\overline{P}_{9,4}$ and $\overline{IP}_{9,4}$ according to equations (16) – (18) and (23) – (25) respectively.

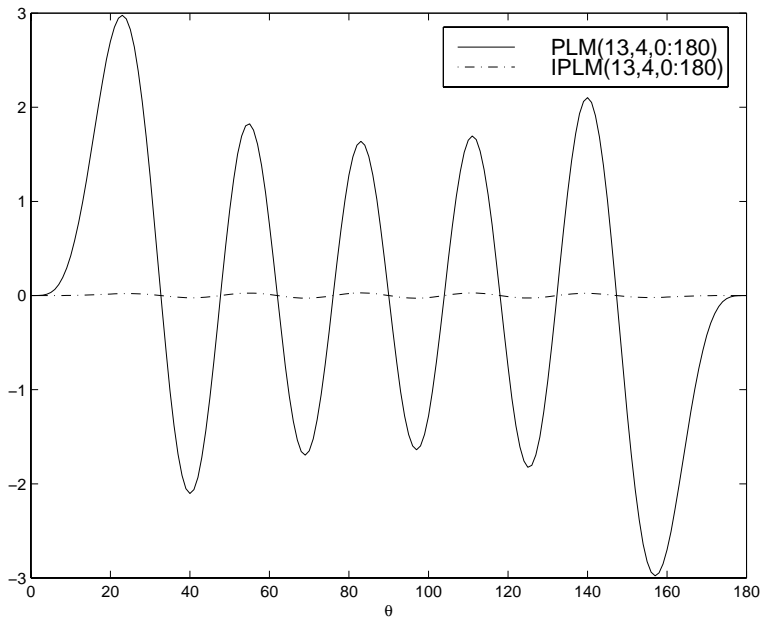


Figure 3: $\bar{P}_{13,4}$ vs. $\bar{I}P_{13,4}$ for $\theta = 0, \pi/180, 2\pi/180, \dots, \pi$.

B Isostasy in Spherical Harmonics

5 The theory of isostasy

The idea of isostasy emerged from the inconsistency between a non-isostatic Earth model and field measurements of some quantities of the gravity field. In a non-isostatic Earth model mountains are assumed to simply rest on a spherically symmetric Earth and the crust has the same constitution below continents and beneath oceans. Such a model however cannot explain the results obtained from geodetic and astronomical observations taken over the last 200 years: deflections of the vertical observed in mountainous regions were less than a non-isostatic Earth would suggest while Bouguer gravity anomalies are systematically negative in mountain areas and positive at sea. These observations led to the theory of isostasy: there should exist mass deficiencies below continents and mass surpluses beneath oceans. The way these density anomalies are distributed is based on the hypothesis of an isostatic equilibrium: below a certain depth which is called the compensation depth, pressures will everywhere be hydrostatic. Two of the most popular, though idealized isostatic models, will be considered in the sequel: the Airy/Heiskanen and the Pratt/Hayford model.

5.1 The Airy/Heiskanen isostatic model

The principle of the Airy/Heiskanen model is illustrated by Fig. 5. The crust is of constant density ($\rho_{cr} = 2.67 \text{ g cm}^{-3}$) but of variable thickness, where highly elevated terrain is compensated by thick crust and low terrain or oceans by thin crust. The density of the denser mantle layer on which the mountains float is considered also of having a constant value, namely $\rho_m = 3.27 \text{ g cm}^{-3}$. Thus the

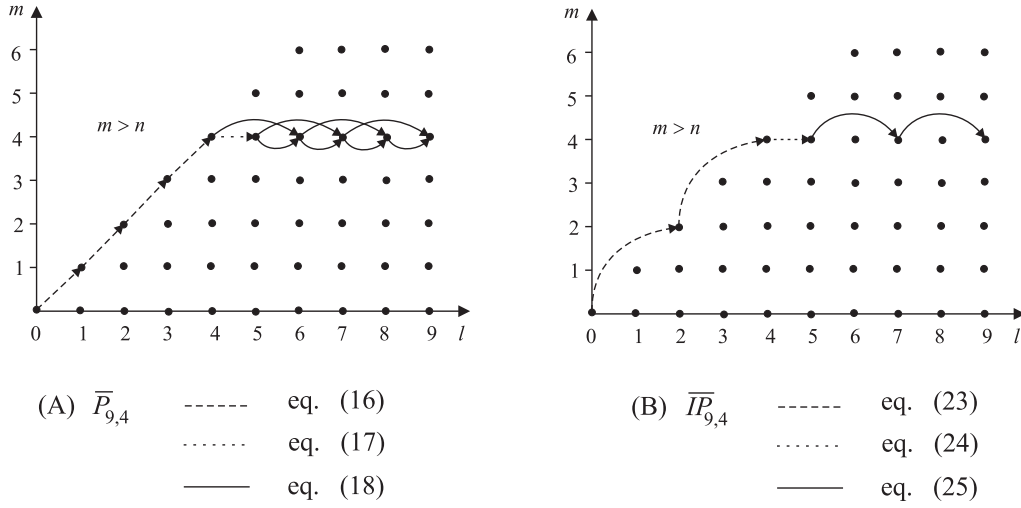


Figure 4: Recursion scheme for the computation of (A) $\bar{P}_{9,4}$ and (B) $\bar{I}\bar{P}_{9,4}$.

density contrast between crust and mantle becomes $\Delta\rho = \rho_m - \rho_{cr} = 0.6 \text{ g cm}^{-3}$. A relation for the variable root (t) and anti-root (t') thickness can be obtained from the condition of floating equilibrium for the continents and the oceans, respectively. For a flat Earth these relations read respectively

$$t\Delta\rho = h\rho_{cr} \quad (29)$$

and

$$t'\Delta\rho = h'(\rho_{cr} - \rho_w) \quad (30)$$

with $\rho_w = 1.03 \text{ g cm}^{-3}$ the density of sea water. When a spherical Earth model is used, i.e. when the convergence of the verticals is taken into account, one has spherical columns instead of rectangular prisms. In this case equations (29) – (30) should be written, respectively, in the form

$$\iint_{\sigma} \int_{r=R-D-t}^{R-D} \Delta\rho r^2 dr d\sigma = \iint_{\sigma} \int_{r=R}^{R+h} \rho_{cr} r^2 dr d\sigma \quad (31)$$

and

$$\iint_{\sigma} \int_{r=R-D}^{R-D+t'} \Delta\rho r^2 dr d\sigma = \iint_{\sigma} \int_{r=R-h'}^R (\rho_{cr} - \rho_w) r^2 dr d\sigma, \quad (32)$$

where R denotes a mean Earth radius ($R = 6370 \text{ km}$) and D is the thickness of the crust for zero elevation. A popular value for D in Airy's model is $D = 30 \text{ km}$. Solving (29) and (30) for t and t' respectively, yields

$$t = \frac{\rho_{cr}}{\Delta\rho} h \quad (33)$$

and

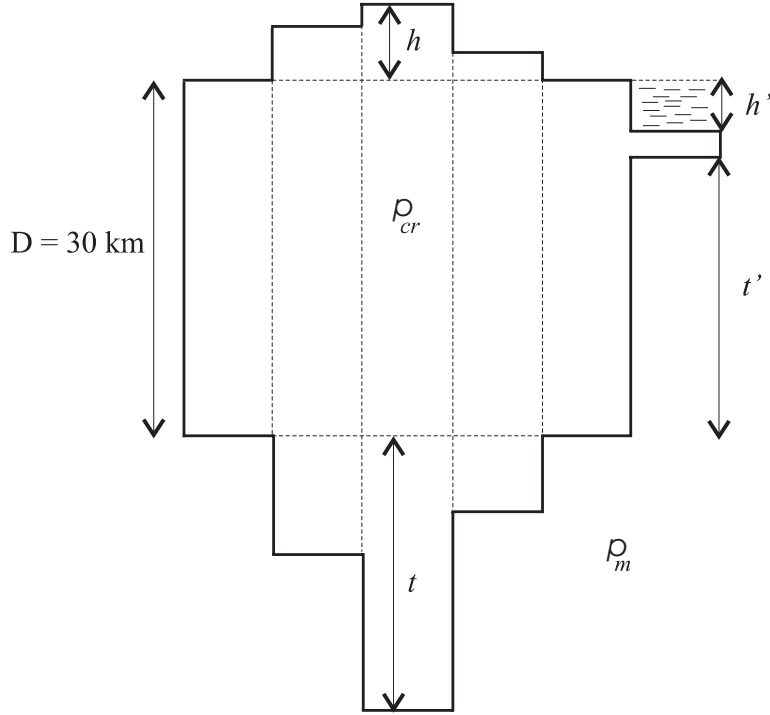


Figure 5: The Airy/Heiskanen isostatic model.

$$t' = \frac{(\rho_{cr} - \rho_w)}{\Delta\rho} h' . \quad (34)$$

The solutions of (31) and (32) in linear approximation are, respectively, (Rummel et al 1988; Lambeck 1988)

$$t = \left(\frac{R}{R - D} \right)^2 \frac{\rho_{cr}}{\Delta\rho} h \quad (35)$$

and

$$t' = \left(\frac{R}{R - D} \right)^2 \frac{(\rho_{cr} - \rho_w)}{\Delta\rho} h' . \quad (36)$$

5.2 The Pratt/Hayford isostatic model

The principle of the Pratt/Hayford isostatic model is illustrated in Fig. 6. Below the level of compensation ($D = 100$ km) there is uniform density ρ_m . Above, floats a layer of thickness $D + h$ or $D - h'$ relative to sea-level and of variable density, so that the mass of each column of the same cross section is constant. Consequently mountains are underlain by low density crust and oceans by high density material. For a flat Earth approximation the density ρ of a column of height $D + h$ (h representing the height of the topography) will satisfy the equation

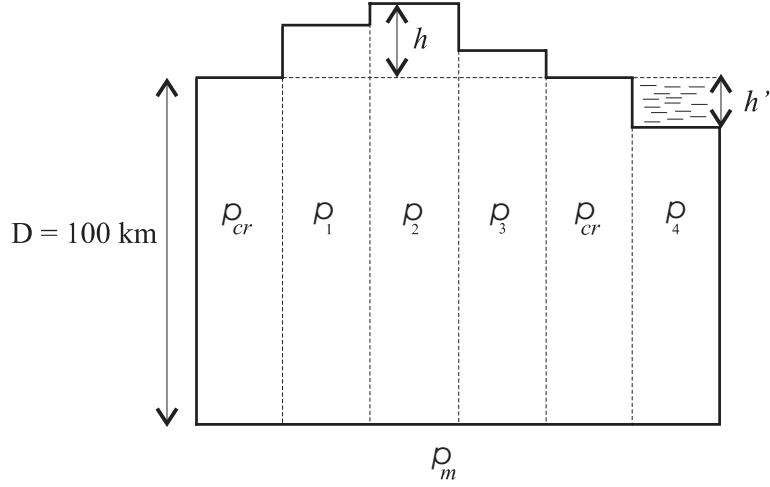


Figure 6: The Pratt/Hayford isostatic model.

$$(D + h) \rho = D \rho_{cr} . \quad (37)$$

Here it is assumed that the density of a column of thickness D equals the density of the crust ρ_{cr} . The variable density underlying the continents in a flat and a spherical Earth is defined respectively as (Lambeck, 1988)

$$\rho = \frac{D}{D + h} \rho_{cr} \quad \text{and} \quad \rho = \left(\frac{R}{R - D} \right)^2 \frac{D}{D + h} \rho_{cr} . \quad (38)$$

For the ocean part we have respectively

$$\rho = \frac{D \rho_{cr} - h' \rho_w}{D - h'} \quad \text{and} \quad \rho = \left(\frac{R}{R - D} \right)^2 \frac{D \rho_{cr} - h' \rho_w}{D - h'} . \quad (39)$$

Hence the mass deficiency in continental regions in a flat and spherical column approximation is given respectively by

$$\Delta \rho^L = \rho_{cr} - \rho = \frac{h}{D + h} \rho_{cr} \quad (40)$$

and, after some reordering,

$$\Delta \rho^L = \rho_{cr} - \rho = \frac{h}{D + h} \rho_{cr} + \frac{D^2(D - 2R)}{(R - D)^2(D + h)} \rho_{cr} . \quad (41)$$

Similarly, the mass surplus for the sub-oceanic columns in both approximations is

$$\Delta \rho^O = \rho - \rho_{cr} = \frac{h'}{D - h'} (\rho_{cr} - \rho_w) \quad (42)$$

and

$$\Delta \rho^O = \rho - \rho_{cr} = \left(\frac{R}{R - D} \right)^2 \frac{h'}{D - h'} (\rho_{cr} - \rho_w) - \frac{(D^2 - 2RD)}{(R - D)^2} \rho_{cr} . \quad (43)$$

6 Topographic/isostatic potential harmonic coefficients using the Airy/Heiskanen model

In the sequel, an algorithm is presented for the computation of the dimensionless potential coefficients \overline{C}_{lm} and \overline{S}_{lm} from a global elevation set. The method is based on a series expansion of the inverse distance function - the kernel function of the Newtonian potential. The isostatic compensation of topography, presented in the previous chapter, is also taken into account. Both isostatic models, Airy/Heiskanen and Pratt/Hayford, are therefore considered. We start by writing down some standard definitions. The gravitational potential at a point P outside the Earth Σ is given by Newton's law of gravitation

$$V(P) = G \iiint_{\Sigma} \frac{\rho(Q)}{l_{PQ}} d\Sigma_Q \quad (44)$$

where G is the gravitational constant, ρ the density inside the Earth and l_{PQ} the distance between P and the infinitesimal volume element $d\Sigma_Q$ at Q . The series expansion for the inverse distance $1/l_{PQ}$ in spherical coordinates is as follows

$$\frac{1}{l_{PQ}} = \frac{1}{r_P} \sum_{l=0}^{\infty} \left(\frac{r_Q}{r_P} \right)^l P_l(\cos \psi_{PQ}) \quad \text{for } r_Q < r_P \quad (45a)$$

$$\frac{1}{l_{PQ}} = \frac{1}{r_Q} \sum_{l=0}^{\infty} \left(\frac{r_P}{r_Q} \right)^l P_l(\cos \psi_{PQ}) \quad \text{for } r_P < r_Q \quad (45b)$$

where $P_l(\cos \psi_{PQ})$ are the Legendre polynomials of degree l and ψ_{PQ} the angle linking Q to the computation point P . Equations (45a) and (45b) indicate a convergency issue: (45a) is valid or convergent for a point P outside a sphere including all masses (Brillouin sphere) while (45b) holds for any point inside a spherical mass layer. For all computations made in the sequel we will refer to a computation point outside or on the Brillouin sphere, i.e. we consider equation (45a) only. A theoretically correct computation taking place e.g. on the geoid demands a combined use of equations (45a) and (45b) and will be considered elsewhere. A separation of the functions related to point P from those related to Q can be made by means of the *addition theorem of the spherical harmonic functions*

$$P_l(\cos \psi_{PQ}) = \frac{1}{2l+1} \sum_{m=0}^l \overline{P}_{lm}(\cos \theta_P) \overline{P}_{lm}(\cos \theta_Q) (\cos m\lambda_P \cos m\lambda_Q + \sin m\lambda_P \sin m\lambda_Q) . \quad (46)$$

Inserting (46) and (45a) in (44) we obtain for the potential the expression

$$V(P) = \frac{GM}{R} \sum_{l=0}^{\infty} \sum_{m=0}^l \left(\frac{R}{r_P} \right)^{l+1} \overline{P}_{lm}(\cos \theta_P) \left(\cos m\lambda_P \overline{C}_{lm} + \sin m\lambda_P \overline{S}_{lm} \right) \quad (47)$$

with the dimensionless coefficients

$$\left. \begin{array}{l} \overline{C}_{lm} \\ \overline{S}_{lm} \end{array} \right\} = \frac{3}{\overline{\rho} R^3 (2l+1)} \frac{1}{4\pi} \iiint_{\Sigma} \left(\frac{r_Q}{R} \right)^l \rho(Q) \overline{P}_{lm}(\cos \theta_Q) \left\{ \begin{array}{l} \cos m\lambda_Q \\ \sin m\lambda_Q \end{array} \right\} d\Sigma_Q . \quad (48)$$

In the last equations the mass of the Earth is introduced, $M = 4/3\pi\bar{\rho}R^3$ in spherical approximation, where $\bar{\rho}$ is a mean density value, e.g. 5.5 g cm^{-3} . Equation (48) is the basic equation for both isostatic models. First we consider the Airy/Heiskanen model. The coefficients derived from the potential of an Airy-compensated topography will be given as the difference between those generated by the potential of the surface topography part and those generated by the compensation part. After introducing in (44) the volume element in spherical coordinates $d\Sigma_Q = r_Q^2 dr_Q d\sigma_Q$ one can write

$$\left. \begin{array}{l} \overline{C}_{lm}^I \\ \overline{S}_{lm}^I \end{array} \right\} = \frac{3}{\bar{\rho}R(2l+1)} \frac{1}{4\pi} \iint_{\sigma} [A^T(Q) - A^C(Q)] \overline{P}_{lm}(\cos\theta_Q) \begin{Bmatrix} \cos m\lambda_Q \\ \sin m\lambda_Q \end{Bmatrix} d\sigma_Q, \quad (49)$$

where the surface topography part is

$$A^T(Q) = \rho_{cr} \int_{r=R}^{R+h} \left(\frac{r_Q}{R}\right)^{l+2} dr_Q \quad (50)$$

and the compensation part

$$A^C(Q) = \Delta\rho \int_{r=R-D-t}^{R-D} \left(\frac{r_Q}{R}\right)^{l+2} dr_Q, \quad (51)$$

with ρ_{cr} the density of the crust and $\Delta\rho = \rho_m - \rho_{cr}$ the density contrast between crust and mantle. Integrating with respect to r_Q yields

$$A^T(Q) = \rho_{cr} \frac{R}{l+3} \left[\left(\frac{R+h(Q)}{R}\right)^{l+3} - 1 \right] \quad (52)$$

and

$$A^C(Q) = \Delta\rho \frac{R}{l+3} \left[\left(\frac{R-D}{R}\right)^{l+3} - \left(\frac{R-D-t(Q)}{R}\right)^{l+3} \right]. \quad (53)$$

In practical computations we replace ocean depths h' in the global elevation set by *equivalent rock topography*. The latter is the height of a column of crustal rock corresponding to the density contrast of the respective oceanic column, i.e.

$$h_{eq} \rho_{cr} = h' (\rho_{cr} - \rho_w) \Rightarrow \begin{cases} h_{eq} = \frac{(\rho_{cr} - \rho_w)}{\rho_{cr}} h' \\ h' = \frac{\rho_{cr}}{(\rho_{cr} - \rho_w)} h_{eq} \end{cases}. \quad (54)$$

The introduction of equivalent rock topography simplifies the computation of the compensation part (53). We recall that $t(Q)$ is computed according to equation (35) for the continental part and by means of (36) for the oceanic part of the global elevation model. Inserting h' from equation (54) into (36) yields

$$t' = \left(\frac{R}{R-D}\right)^2 \frac{(\rho_{cr} - \rho_w)}{\Delta\rho} \frac{\rho_{cr}}{(\rho_{cr} - \rho_w)} h_{eq} = \left(\frac{R}{R-D}\right)^2 \frac{\rho_{cr}}{\Delta\rho} h_{eq} \equiv t. \quad (55)$$

Thus, using equivalent rock topography permits the use of equation (35) for the computation of the root as well as the anti-root thickness. Expanding the expressions in brackets of equations (52) and (53) in a binomial series and inserting t from (35) into (53) one obtains after a few steps the following series expression for the potential coefficients of the uncompensated topography (for derivations, see Rummel et al. 1988)

$$\left. \begin{array}{l} \overline{C}_{lm}^T \\ \overline{S}_{lm}^T \end{array} \right\} = \frac{3}{2l+1} \frac{\rho_{cr}}{\bar{\rho}} \left\{ h_{lm} + \frac{l+2}{2} h_{2lm} + \frac{(l+2)(l+1)}{6} h_{3lm} \right\} . \quad (56)$$

Doing the same with equation (53), inserting t from (35), the coefficients of the isostatic compensation will be

$$\left. \begin{array}{l} \overline{C}_{lm}^C \\ \overline{S}_{lm}^C \end{array} \right\} = \frac{3}{2l+1} \frac{\rho_{cr}}{\bar{\rho}} \left\{ \left(\frac{R-D}{R} \right)^l h_{lm} - \frac{l+2}{2} \frac{\rho_{cr}}{\Delta\rho} \left(\frac{R-D}{R} \right)^{l-3} h_{2lm} \right. \\ \left. + \frac{(l+2)(l+1)}{6} \frac{\rho_{cr}^2}{\Delta\rho^2} \left(\frac{R-D}{R} \right)^{l-6} h_{3lm} \right\} . \quad (57)$$

Finally, the coefficients of the isostatically compensated topography will be given by

$$\left\{ \begin{array}{l} \overline{C}_{lm}^I \\ \overline{S}_{lm}^I \end{array} \right\} = \left\{ \begin{array}{l} \overline{C}_{lm}^T \\ \overline{S}_{lm}^T \end{array} \right\} - \left\{ \begin{array}{l} \overline{C}_{lm}^C \\ \overline{S}_{lm}^C \end{array} \right\} . \quad (58)$$

For a shorter notation we introduced the surface harmonic expansions

$$h_{lm} = \frac{1}{4\pi} \iint_{\sigma} \frac{h(Q)}{R} \overline{P}_{lm}(\cos\theta_Q) \left\{ \begin{array}{l} \cos m\lambda_Q \\ \sin m\lambda_Q \end{array} \right\} d\sigma_Q , \quad (59)$$

$$h_{2lm} = \frac{1}{4\pi} \iint_{\sigma} \frac{h^2(Q)}{R^2} \overline{P}_{lm}(\cos\theta_Q) \left\{ \begin{array}{l} \cos m\lambda_Q \\ \sin m\lambda_Q \end{array} \right\} d\sigma_Q \quad (60)$$

and

$$h_{3lm} = \frac{1}{4\pi} \iint_{\sigma} \frac{h^3(Q)}{R^3} \overline{P}_{lm}(\cos\theta_Q) \left\{ \begin{array}{l} \cos m\lambda_Q \\ \sin m\lambda_Q \end{array} \right\} d\sigma_Q . \quad (61)$$

In the left hand side of equations (59) – (61) no distinction between the sin and the cos - coefficients is made in the applied notation. The reason is that h_{lm} , h_{2lm} and h_{3lm} represent $(L+1) \times (L+1)$ matrices which comprise both the \overline{C}_{lm} and \overline{S}_{lm} coefficients written in the so-called —C§— format. For a first presentation of the numerical results the potential coefficient spectrum was computed. The degree variance (spectral power or simply spectrum) of a set of coefficients for degree l is defined by

$$\sigma_l^2 = \sum_{m=0}^l (\overline{C}_{lm}^2 + \overline{S}_{lm}^2) . \quad (62)$$

Fig. 7 displays the separate contribution of h_{lm} , h_{2lm} and h_{3lm} to the computation of the uncompensated potential coefficients according to equation (56). The h_{lm} 's are properly multiplied by the respective factors given in (56), so that the curves shown eventually in Fig. 7 have dimensions of

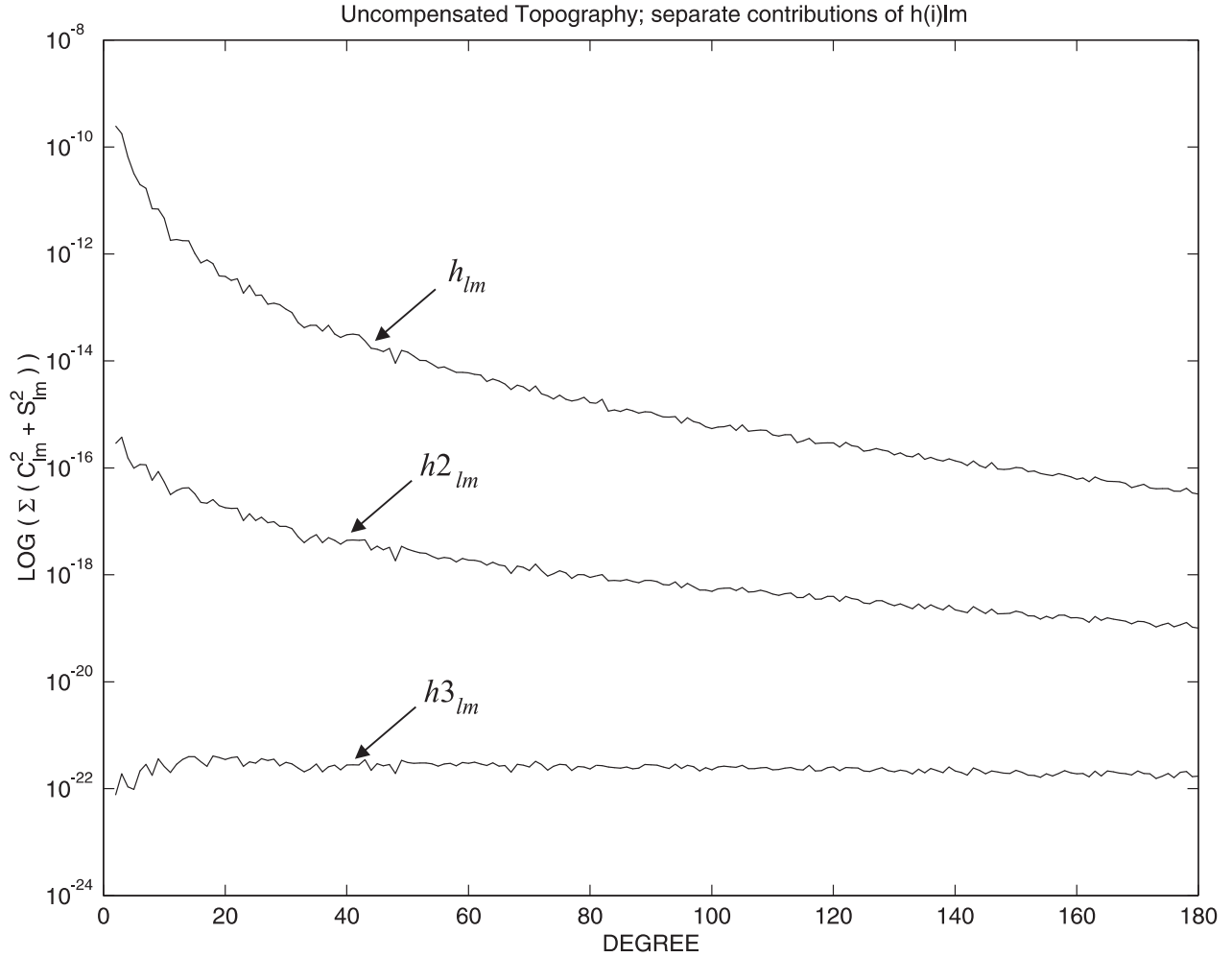


Figure 7: Separate contributions of h_{lm} , $h2_{lm}$ and $h3_{lm}$ (eqs. (59) – (61)) to the computation of the uncompensated potential coefficients (eq. 56).

$\sigma_l^2 = \sum_{m=0}^l \left((\overline{C}_{lm}^T)^2 + (\overline{S}_{lm}^T)^2 \right)$. These computations agree with those reported in Rummel et al (1988): The power spectra of $(h/R)^2$ and $(h/R)^3$ are approximately 10^{-6} and 10^{-13} , respectively, of the power of (h/R) . Fig. 8 compares the uncompensated, the compensated after Airy and the truncated up to maximum degree and order 180 potential coefficient spectrum of EGM96. In all representations, displayed are the degree variances σ_l^2 for degree $l \geq 2$; the zeroth and first degree of the spectrum deserves a separate discussion which will be done elsewhere.

7 Topographic/isostatic potential harmonic coefficients using the Pratt/Hayford model

For the Pratt/Hayford model a procedure similar to the one shown in the previous section will be applied. Here, the surface topography part equals the attraction of the oceans assuming for simplicity

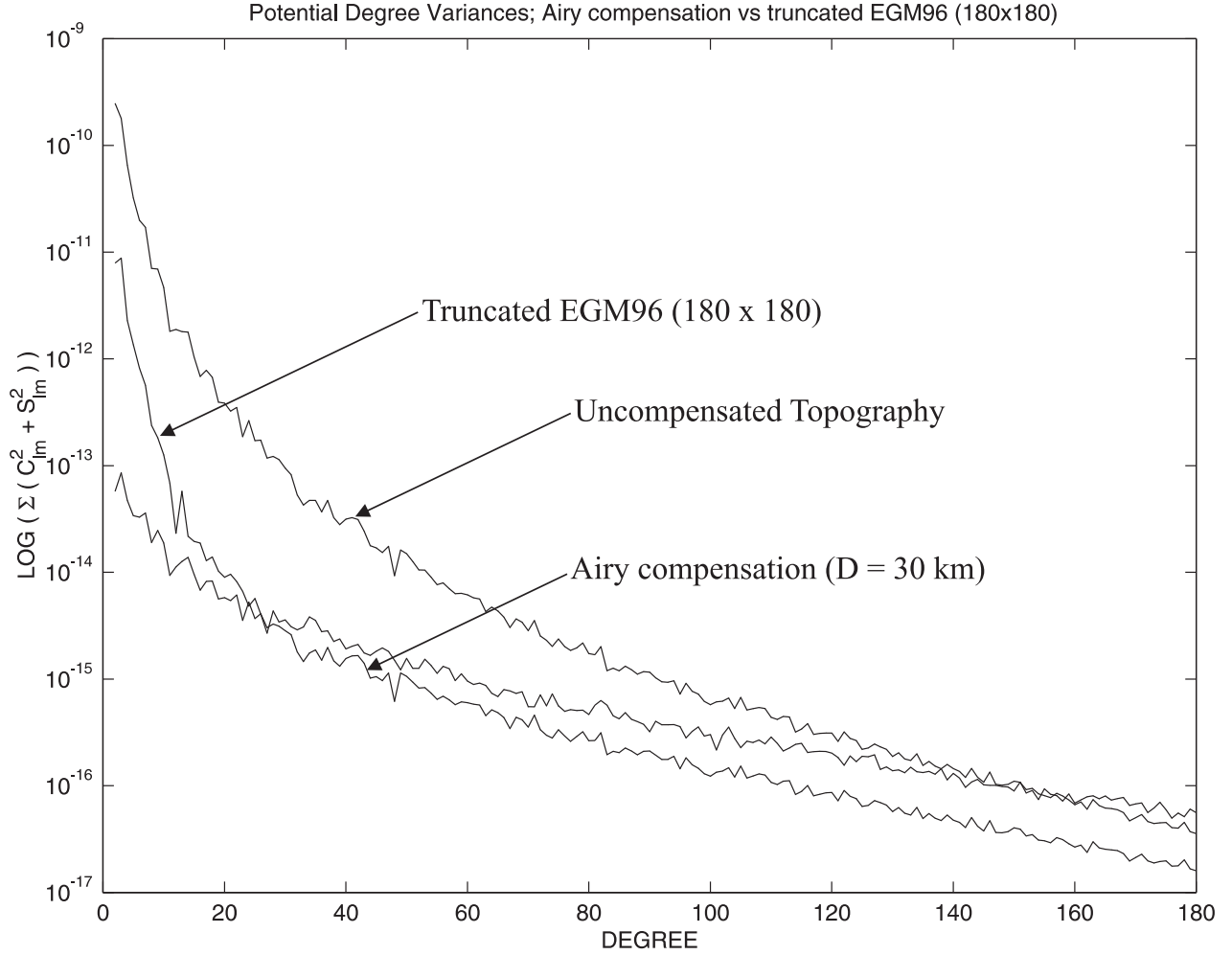


Figure 8: A comparison between the following potential coefficient spectra: uncompensated topography, eq. (56), isostatically compensated topography after Airy, eq. (57) and the truncated (180×180) EGM96 model.

reasons that the density remains constant and equal to ρ_w . The compensation part corresponds to the potential generated by the variable density anomalies (40) – (43). Thus, the topographic/isostatic coefficients using the Pratt/Hayford model will be given by rewriting equations (49) – (51)

$$\left. \begin{array}{l} \overline{C}_{lm}^I \\ \overline{S}_{lm}^I \end{array} \right\} = \frac{3}{\overline{\rho}R(2l+1)} \frac{1}{4\pi} \iint_{\sigma} [A^T(Q) - A^C(Q)] \overline{P}_{lm}(\cos \theta_Q) \begin{Bmatrix} \cos m\lambda_Q \\ \sin m\lambda_Q \end{Bmatrix} d\sigma_Q, \quad (63)$$

where

$$A^T(Q) = \int_{r=R-h'}^R \left(\frac{r_Q}{R}\right)^{l+2} \rho_w dr_Q, \quad (64a)$$

$$A^C(Q) = \begin{cases} \int_{r=R-D}^{R+h} \left(\frac{r_Q}{R}\right)^{l+2} \Delta^L \rho(Q) dr_Q & \text{LAND PART} \\ \int_{r=R-D}^{R-h'} \left(\frac{r_Q}{R}\right)^{l+2} \Delta^O \rho(Q) dr_Q & \text{OCEAN PART} \end{cases} \quad (64b)$$

and $\Delta^L \rho(Q)$, $\Delta^O \rho(Q)$ denote the density anomalies beneath continents and oceans respectively and are given by equations (40) – (41) and (42) – (43) depending on whether the convergence of the verticals is taken into consideration or not.

At first we derive a series expansion for equation (64a). Integrating with respect to r_Q one gets

$$A^T(Q) = \rho_w \frac{R}{l+3} \left[\left(\frac{r_Q}{R}\right)^{l+3} \right]_{R-h'}^R = \rho_w \frac{R}{l+3} \left[1 - \left(\frac{R-h'}{R}\right)^{l+3} \right]. \quad (65)$$

Expanding the second term in the bracket into a binomial series up to third order in h'/R yields

$$A^T(Q) = \rho_w R \left[\frac{h'}{R} - \frac{l+2}{2} \left(\frac{h'}{R}\right)^2 + \frac{(l+2)(l+1)}{6} \left(\frac{h'}{R}\right)^3 \right]. \quad (66)$$

We proceed now to the computation of (64b); for simplicity reasons we neglect at first the effect of the convergence of the verticals. Expressions taking into account the convergence of the columns will be derived afterwards. For a ‘flat’ column, inserting equation (40) into the first equation of (64b) yields

$$\begin{aligned} A_{\text{LAND}}^C(Q) &= \int_{r=R-D}^{R+h} \left(\frac{r_Q}{R}\right)^{l+2} \frac{h}{D+h} \rho_{cr} dr_Q \\ &= \frac{h}{D+h} \rho_{cr} \frac{R}{l+3} \left[\left(\frac{r_Q}{R}\right)^{l+3} \right]_{R-D}^{R+h} \\ &= \frac{h}{D+h} \rho_{cr} \frac{R}{l+3} \left[\left(\frac{R+h}{R}\right)^{l+3} - \left(\frac{R-D}{R}\right)^{l+3} \right] \end{aligned} \quad (67)$$

Expanding the first term in the bracket of equation (67) into a binomial expansion yields up to third order in h/R

$$\begin{aligned} A_{\text{LAND}}^C(Q) &= \frac{h}{D+h} \rho_{cr} \frac{R}{l+3} \left[1 + (l+3) \frac{h}{R} + \frac{(l+3)(l+2)}{2} \left(\frac{h}{R}\right)^2 + \right. \\ &\quad \left. + \frac{(l+3)(l+2)(l+1)}{6} \left(\frac{h}{R}\right)^3 - \left(\frac{R-D}{R}\right)^{l+3} \right] \\ &= \frac{h}{D+h} \rho_{cr} h \left[1 + \frac{l+2}{2} \frac{h}{R} + \frac{(l+2)(l+1)}{6} \left(\frac{h}{R}\right)^2 \right] + \end{aligned}$$

$$+ \frac{h}{D+h} \rho_{cr} \frac{R}{l+3} \left[1 - \left(\frac{R-D}{R} \right)^{l+3} \right] . \quad (68)$$

Inserting (42) into the second equation of (64b) and following the steps shown in equations (67) – (68) we obtain similarly for the ocean part

$$\begin{aligned} A_{\text{OCEAN}}^{\text{C}}(Q) &= \frac{h'}{D-h'} (\rho_{cr} - \rho_w) h' \left[-1 + \frac{l+2}{2} \frac{h'}{R} - \frac{(l+2)(l+1)}{6} \left(\frac{h'}{R} \right)^2 \right] + \\ &+ \frac{h'}{D-h'} (\rho_{cr} - \rho_w) \frac{R}{l+3} \left[1 - \left(\frac{R-D}{R} \right)^{l+3} \right] . \end{aligned} \quad (69)$$

Here, h' denotes the bathymetry information, i.e. the original depths of the global elevation set taken in absolute value; the concept of equivalent rock topography is absent in the analysis of the Pratt isostatic model followed here. Inserting expressions (66), (68) and (69) into equation (63) we obtain respectively a separate contribution from the topography part, the land and the ocean isostatic part to the potential coefficients, due to an isostatically compensated topography after Pratt. For ‘flat’ columns we have respectively

$$\left. \begin{array}{l} \overline{C}_{lm}^{\text{T}} \\ \overline{S}_{lm}^{\text{T}} \end{array} \right\} = \frac{\rho_w}{\bar{\rho}} \frac{3}{2l+1} \left\{ h'_{lm} - \frac{l+2}{2} h'_{2lm} + \frac{(l+2)(l+1)}{6} h'_{3lm} \right\} , \quad (70)$$

$$\begin{aligned} \left. \begin{array}{l} \overline{C}_{lm}^{\text{LAND}} \\ \overline{S}_{lm}^{\text{LAND}} \end{array} \right\} &= \frac{\rho_{cr}}{\bar{\rho}} \frac{3}{2l+1} \left\{ h_{lm} + \frac{l+2}{2} h_{2lm} + \frac{(l+2)(l+1)}{6} h_{3lm} \right\} + \\ &+ \frac{\rho_{cr}}{\bar{\rho}} \frac{3}{(2l+1)(l+3)} \left[1 - \left(\frac{R-D}{R} \right)^{l+3} \right] h_{dh} \end{aligned} \quad (71)$$

and

$$\begin{aligned} \left. \begin{array}{l} \overline{C}_{lm}^{\text{OCEAN}} \\ \overline{S}_{lm}^{\text{OCEAN}} \end{array} \right\} &= \frac{(\rho_{cr} - \rho_w)}{\bar{\rho}} \frac{3}{2l+1} \left\{ -h''_{lm} + \frac{l+2}{2} h''_{2lm} - \frac{(l+2)(l+1)}{6} h''_{3lm} \right\} + \\ &+ \frac{(\rho_{cr} - \rho_w)}{\bar{\rho}} \frac{3}{(2l+1)(l+3)} \left[1 - \left(\frac{R-D}{R} \right)^{l+3} \right] h''_{dh} , \end{aligned} \quad (72)$$

where the following surface spherical harmonic expansions have been defined:

$$h_{lm} = \frac{1}{4\pi} \iint_{\sigma} \left(\frac{h}{D+h} \right) \frac{h(Q)}{R} \overline{P}_{lm}(\cos \theta_Q) \left\{ \begin{array}{l} \cos m\lambda_Q \\ \sin m\lambda_Q \end{array} \right\} d\sigma_Q , \quad (73)$$

$$h_{2lm} = \frac{1}{4\pi} \iint_{\sigma} \left(\frac{h}{D+h} \right) \left(\frac{h}{R} \right)^2 \overline{P}_{lm}(\cos \theta_Q) \left\{ \begin{array}{l} \cos m\lambda_Q \\ \sin m\lambda_Q \end{array} \right\} d\sigma_Q , \quad (74)$$

$$h_{3lm} = \frac{1}{4\pi} \iint_{\sigma} \left(\frac{h}{D+h} \right) \left(\frac{h}{R} \right)^3 \overline{P}_{lm}(\cos \theta_Q) \left\{ \begin{array}{l} \cos m\lambda_Q \\ \sin m\lambda_Q \end{array} \right\} d\sigma_Q , \quad (75)$$

$$h_{dh} = \frac{1}{4\pi} \iint_{\sigma} \left(\frac{h}{D+h} \right) \overline{P}_{lm}(\cos \theta_Q) \left\{ \begin{array}{c} \cos m\lambda_Q \\ \sin m\lambda_Q \end{array} \right\} d\sigma_Q , \quad (76)$$

$$h'_{lm} = \frac{1}{4\pi} \iint_{\sigma} \frac{h'}{R} \overline{P}_{lm}(\cos \theta_Q) \left\{ \begin{array}{c} \cos m\lambda_Q \\ \sin m\lambda_Q \end{array} \right\} d\sigma_Q , \quad (77)$$

$$h2'_{lm} = \frac{1}{4\pi} \iint_{\sigma} \left(\frac{h'}{R} \right)^2 \overline{P}_{lm}(\cos \theta_Q) \left\{ \begin{array}{c} \cos m\lambda_Q \\ \sin m\lambda_Q \end{array} \right\} d\sigma_Q , \quad (78)$$

$$h3'_{lm} = \frac{1}{4\pi} \iint_{\sigma} \left(\frac{h'}{R} \right)^3 \overline{P}_{lm}(\cos \theta_Q) \left\{ \begin{array}{c} \cos m\lambda_Q \\ \sin m\lambda_Q \end{array} \right\} d\sigma_Q \quad (79)$$

and

$$h''_{lm} = \frac{1}{4\pi} \iint_{\sigma} \left(\frac{h'}{D-h'} \right) \frac{h'}{R} \overline{P}_{lm}(\cos \theta_Q) \left\{ \begin{array}{c} \cos m\lambda_Q \\ \sin m\lambda_Q \end{array} \right\} d\sigma_Q , \quad (80)$$

$$h2''_{lm} = \frac{1}{4\pi} \iint_{\sigma} \left(\frac{h'}{D-h'} \right) \left(\frac{h'}{R} \right)^2 \overline{P}_{lm}(\cos \theta_Q) \left\{ \begin{array}{c} \cos m\lambda_Q \\ \sin m\lambda_Q \end{array} \right\} d\sigma_Q , \quad (81)$$

$$h3''_{lm} = \frac{1}{4\pi} \iint_{\sigma} \left(\frac{h'}{D-h'} \right) \left(\frac{h'}{R} \right)^3 \overline{P}_{lm}(\cos \theta_Q) \left\{ \begin{array}{c} \cos m\lambda_Q \\ \sin m\lambda_Q \end{array} \right\} d\sigma_Q , \quad (82)$$

$$h''_{dh} = \frac{1}{4\pi} \iint_{\sigma} \left(\frac{h'}{D-h'} \right) \overline{P}_{lm}(\cos \theta_Q) \left\{ \begin{array}{c} \cos m\lambda_Q \\ \sin m\lambda_Q \end{array} \right\} d\sigma_Q . \quad (83)$$

The final result for the coefficients of the isostatically compensated topography employing the Pratt/Hayford model reads

$$\left\{ \begin{array}{c} \overline{C}_{lm}^I \\ \overline{S}_{lm}^I \end{array} \right\} = \left\{ \begin{array}{c} \overline{C}_{lm}^T \\ \overline{S}_{lm}^T \end{array} \right\} - \left\{ \begin{array}{c} \overline{C}_{lm}^{\text{LAND}} \\ \overline{S}_{lm}^{\text{LAND}} \end{array} \right\} - \left\{ \begin{array}{c} \overline{C}_{lm}^{\text{OCEAN}} \\ \overline{S}_{lm}^{\text{OCEAN}} \end{array} \right\} \quad (84)$$

with equations (70) – (72) representing the individual parts of the right hand side of this equation. In order to use spherical converging columns in the computation of the isostatic part of the coefficients one has to insert equations (41) and (43) into the first and second integral of (64b), respectively. Following the same procedure one is led for the ‘land’ part again to equation (71) with expansions (73) – (76) modified as follows

$$h_{lm} = \frac{1}{4\pi} \iint_{\sigma} \left(\frac{h}{D+h} + \frac{D^2(D-2R)}{(R-D)^2(D+h)} \right) \frac{h(Q)}{R} \overline{P}_{lm}(\cos \theta_Q) \left\{ \begin{array}{c} \cos m\lambda_Q \\ \sin m\lambda_Q \end{array} \right\} d\sigma_Q , \quad (85)$$

the remaining equations being written analogously. In other words, in order to account for the convergence of the verticals in the computation of the ‘land’ part one has to replace the factor

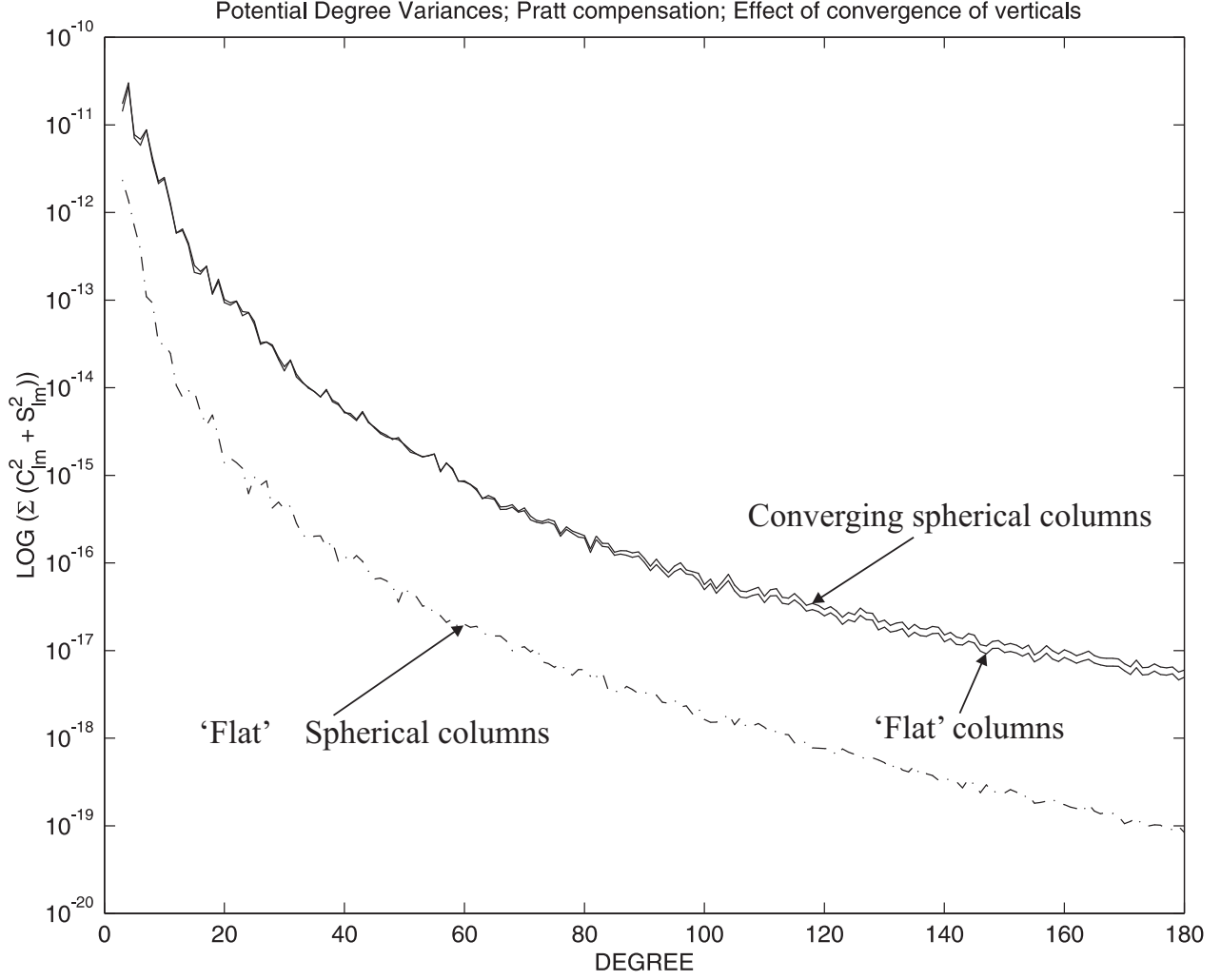


Figure 9: The effect of the convergence of the vertical columns in Pratt's isostatic model.

$h/(D+h)$ in expansions (73) – (76) with equation (41) and then apply equation (71). For the ocean part one obtains the following slightly modified version of expression (72)

$$\left. \begin{array}{l} \overline{C}_{lm}^{\text{OCEAN}} \\ \overline{S}_{lm}^{\text{OCEAN}} \end{array} \right\} = \frac{3}{\bar{\rho}(2l+1)} \left\{ -h''_{lm} + \frac{l+2}{2} h2''_{lm} - \frac{(l+2)(l+1)}{6} h3''_{lm} \right\} + \\ + \frac{3}{\bar{\rho}(2l+1)(l+3)} \left[1 - \left(\frac{R-D}{R} \right)^{l+3} \right] h''_{dh} , \quad (86)$$

with expansions (80) – (83) modified as follows

$$h''_{lm} = \frac{1}{4\pi} \iint_{\sigma} \Delta^O \rho(Q) \frac{h'}{R} \overline{P}_{lm}(\cos \theta_Q) \left\{ \begin{array}{l} \cos m\lambda_Q \\ \sin m\lambda_Q \end{array} \right\} d\sigma_Q , \quad (87)$$

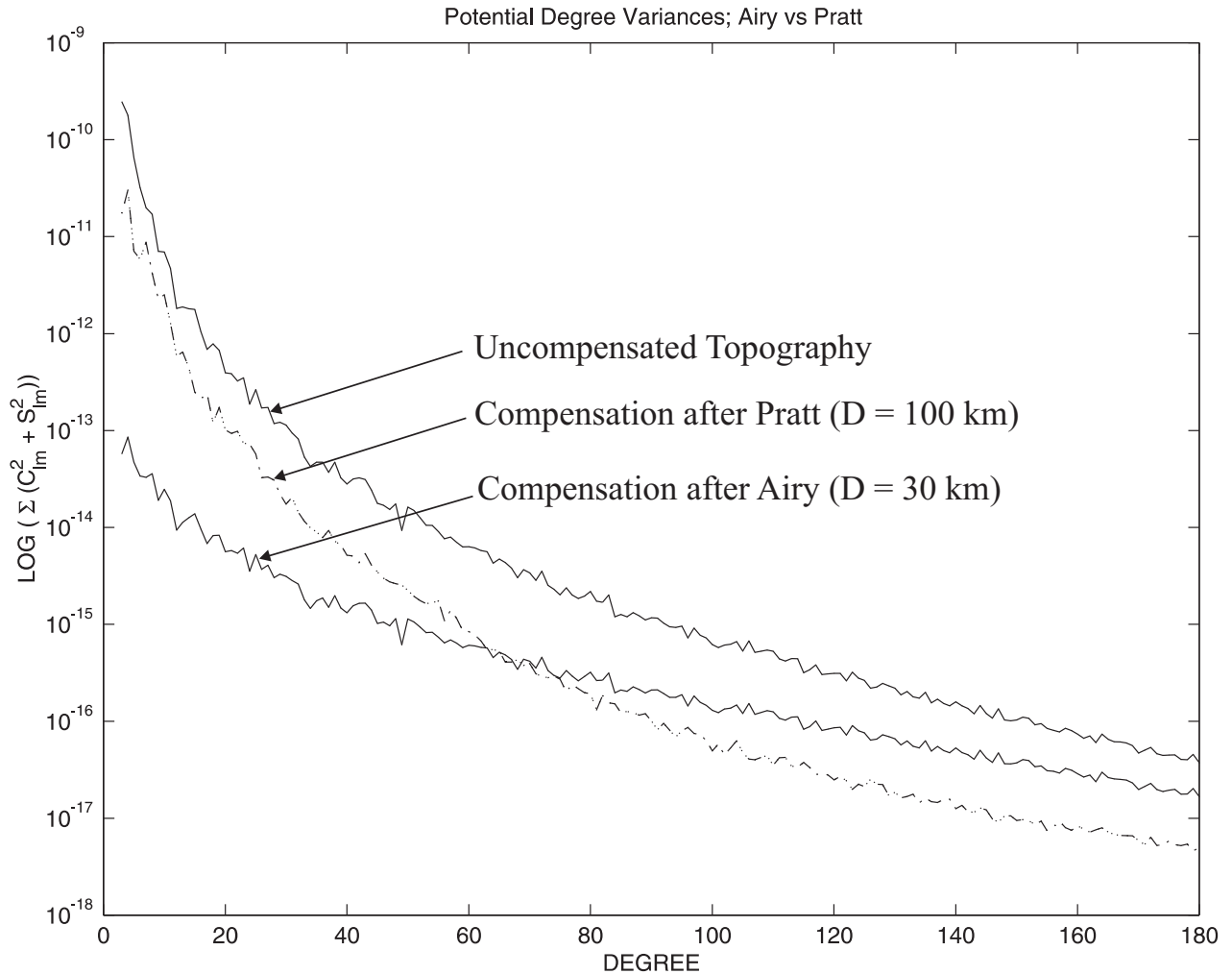


Figure 10: Airy vs Pratt compensation.

$\Delta^O \rho(Q)$ given by (43) and remaining equations ((81) – (83)) being treated in an analogous manner. Thus, for the computation of the contribution to the potential coefficients of the ocean part of the isostatic compensation of a ‘Pratt’-compensated elevation model accounting for the convergence of verticals, expression (86) has to be used. The expansions h''_{lm} , h''_{2lm} , h''_{3lm} and h''_{dh} appearing in (86) can be found from equations (80) – (83) replacing the factor $h'/(D - h')$ by the density anomaly $\Delta^O \rho(Q)$ as given by (43).

Following the spectra computations carried out in the previous section we proceed to analogous computations for the Pratt/Hayford model. Fig. 9 displays the effect of neglecting the convergence of verticals on the power spectra of the respective potential coefficients. Illustrated are the power spectra of the set of coefficients complying to ‘flat’ columns for the isostatic part (equations (70) – (72)), the one with respect to spherically convergent columns ((70) – (72) & (85) – (87)) and the spectrum corresponding to the set of potential coefficients generated by subtracting the two. One sees that the spectrum of this ‘residual’ set of coefficients is approximately 10^{-2} of the power of either the ‘flat’ or the ‘spherical column’ coefficients. Finally, in Fig. 10 both power spectra of Airy and Pratt

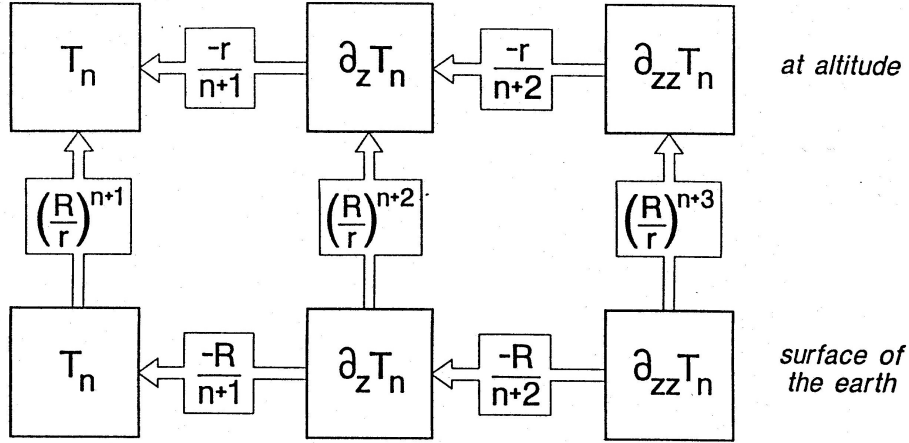


Figure 11: Meissl's spectral scheme (after Rummel and van Gelderen, 1995).

compensation are shown in a single graph. We observe that the latter is 10^{-2} to 10^{-1} times the Airy spectrum, at least up to degree 40. The Pratt spectrum declines more abruptly than the one derived from Airy compensation. The two spectra intersect at degree 70 and from that point up to degree 180 Pratt remains steadily below Airy.

Departing from one of the obtained set of potential coefficients \overline{C}_{lm} and \overline{S}_{lm} one can further compute different functionals of the gravity field in a global as well on a regional scale as will be shown in the following sections.

8 Meissl's spectral scheme

So far only potential coefficients were discussed. We presented two different algorithms of computing a set of coefficients for the Earth's gravitational potential V analyzing a global elevation model. We repeat that this analysis is analogous to an inverse Fourier transform: the elevation set is transformed to the spectral domain into a set of \overline{C}_{lm} and \overline{S}_{lm} . There, by simple multiplication of these coefficients with the appropriate eigenvalues another set of coefficients is obtained which correspond to some desired functional of the gravitational field. This is possible due to the fact that in the spectral domain the disturbing potential ($T = V - U$, U being the reference normal potential) is connected to its first and second order derivatives with some very simple eigenvalues expressions. This simple scheme is known as Meissl's scheme (Rummel 1991; Rummel and van Gelderen 1995) and it enables the determination of any desired 'disturbing' or 'anomalous' gravity quantity. Fig. 11 illustrates Meissl's scheme for the disturbing potential and its first and second derivatives. The arrows indicate the smoothing directions. In opposite directions unsmoothing occurs, i.e. amplification of high frequencies. Smoothing corresponds to integration, i.e. to integral relations in the space domain, while in unsmoothing direction differentiation occurs. For the anomalous quantities (e.g. gravity anomalies dg) one has at first to recall the fundamental equation of physical geodesy which connects Δg , T and T_r . From this equation one is led to the following dimensionless value for the eigenvalue connecting dg and T (Rummel 1991)

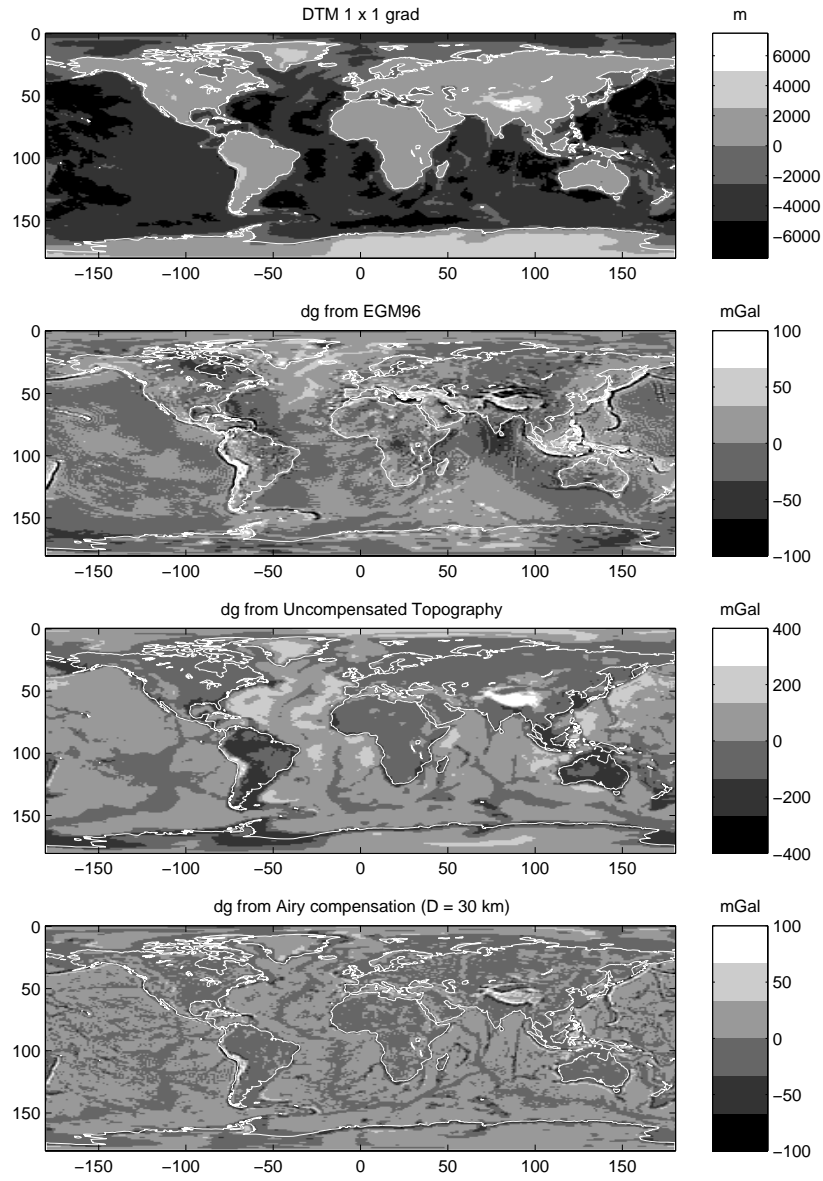


Figure 12: Digital terrain model, gravity anomalies from uncompensated topography, from EGM96 truncated at degree and order 180 and from Airy-compensated topography.

$$\lambda_l (T, dg) = \frac{1}{l - 1} \quad (88)$$

and

$$\lambda_l (dg, T) = (l - 1) . \quad (89)$$

This means, for example, that in order to obtain Δg from T , the coefficients of the latter have only to be multiplied by $(l - 1)$.

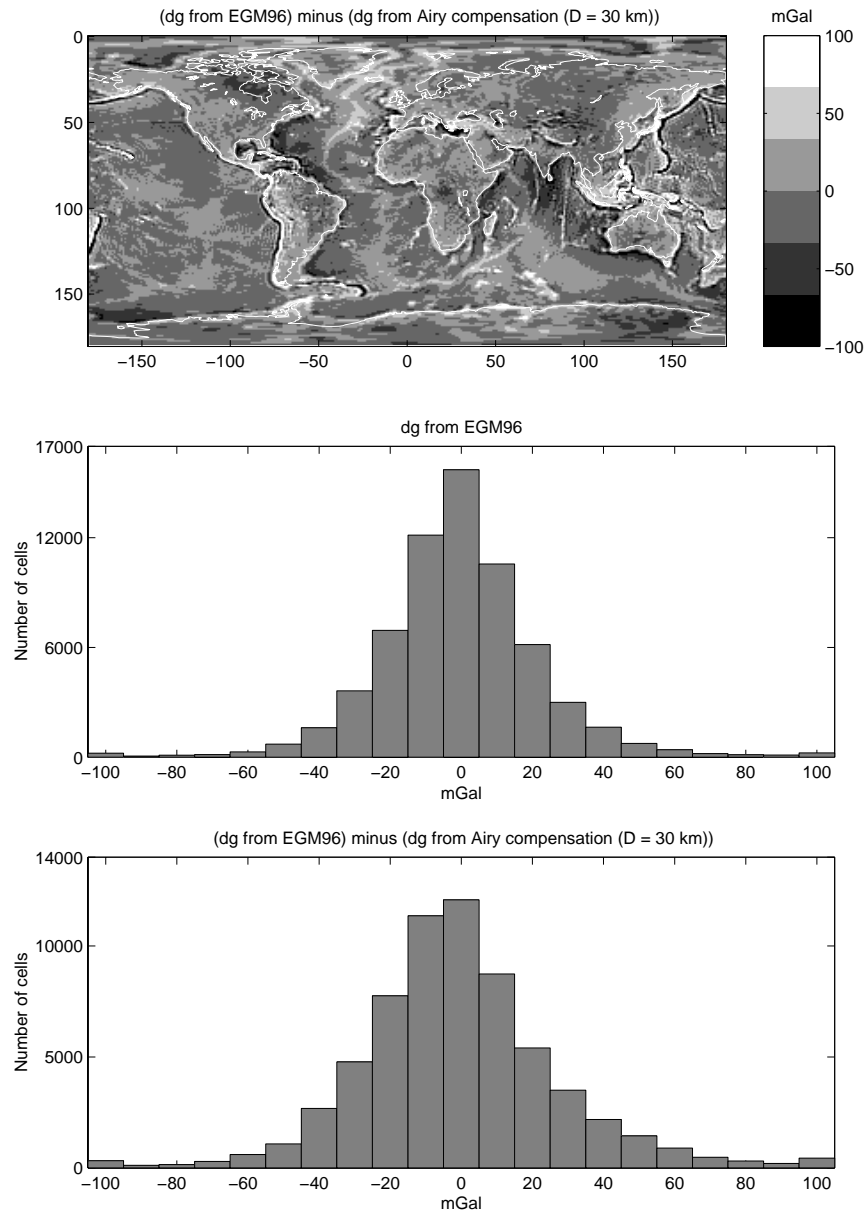


Figure 13: Histogram of differences between EGM96 and Airy compensation.

9 Global Spherical Harmonic Synthesis applications

Using equation (89) one can compute a harmonic set of coefficients which corresponds to gravity anomalies. A direct Fourier transform using this set, i.e. a global spherical harmonic synthesis, will produce a global field of gravity anomalies. For every obtained set of potential harmonic coefficients presented in the previous sections there corresponds a respective set of gravity anomaly coefficients. Thus, we have a Δg set derived from uncompensated topography and a set from Airy and Pratt compensation, respectively. Computing the respective Δg global fields gives a first impression of an

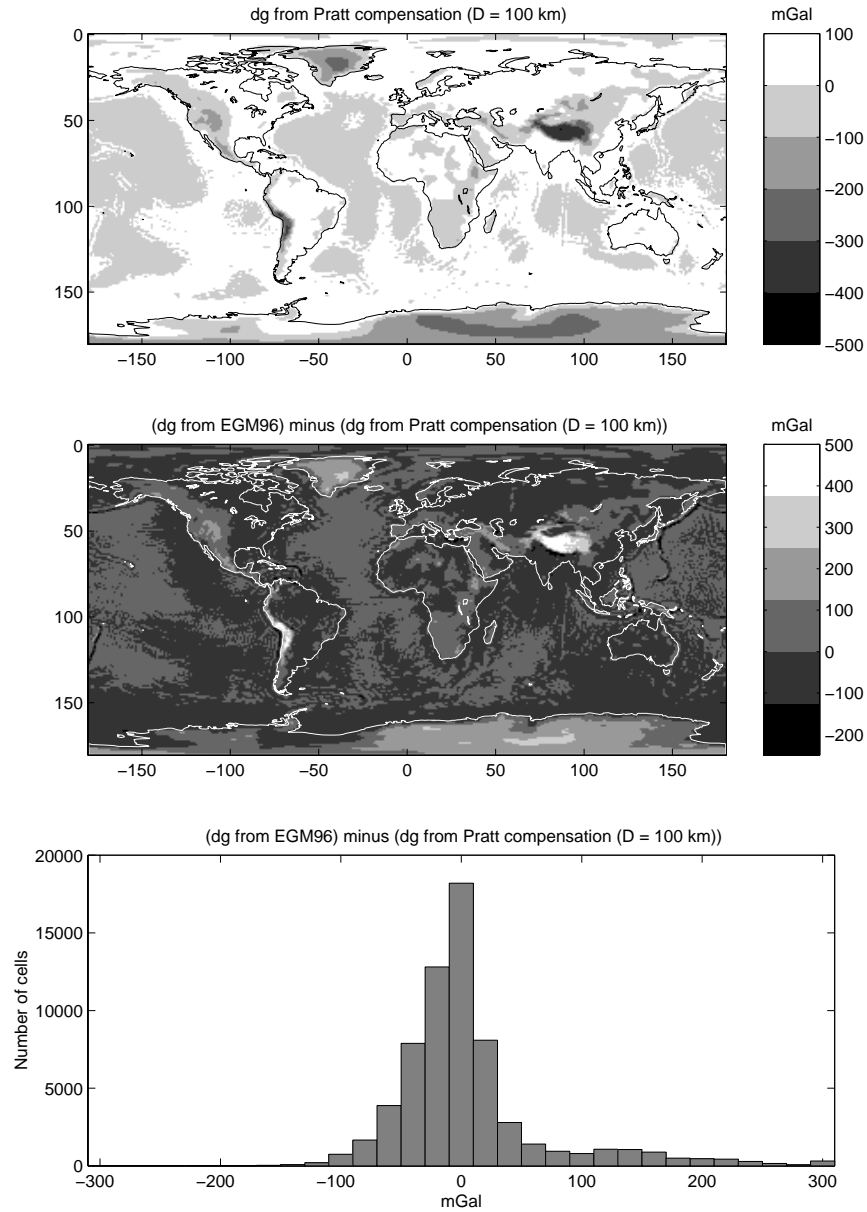


Figure 14: Histogram of differences between EGM96 and Pratt compensation.

uncompensated Δg field, of an *Airy-compensated Δg field* or a *Pratt-compensated Δg field*. In this way the effect of compensation can be investigated in a global sense. Furthermore, these sets can be compared to one of the so called *observed* gravity fields, for example EGM96. This model incorporates different sources of data (from surface gravity data to direct altimeter ranges from TOPEX/POSEIDON, ERS-1 and GEOSAT) and provides a set of potential harmonic coefficients up to degree 360 (Lemoine et al. 1998). Applying the topographic/isostatic coefficients obtained from the theoretical development of the previous sections to the evaluation of a global gravity anomaly field, should give a field that, unlike EGM96 or another *observed* model, reveals terrain structures. In other words, the topographic/isostatic Δg field should be such that the removal of the topographic signal becomes clearly noticeable. Fig. 12 displays the uncompensated Δg field (equations (56) & (89)), that based on

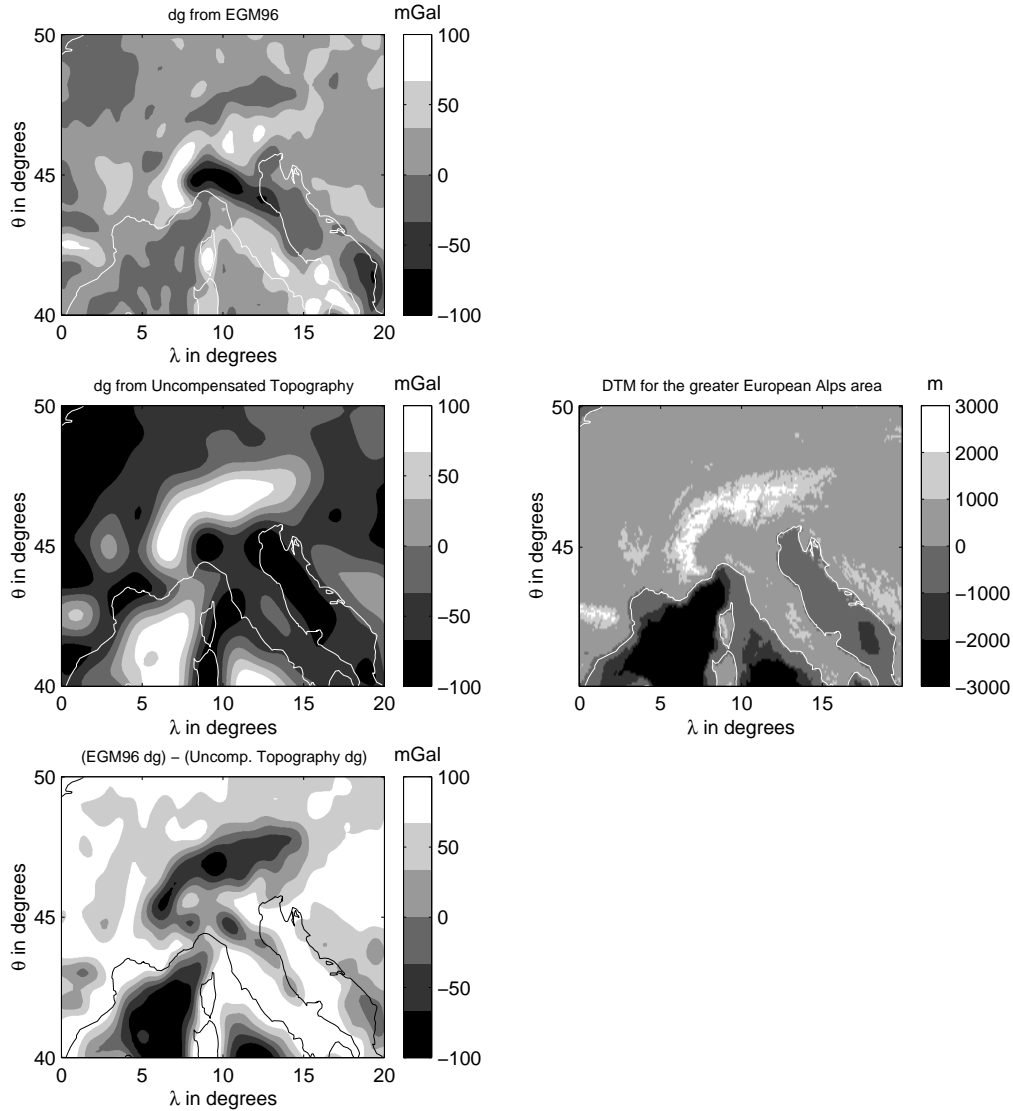


Figure 15: Regional Spherical Harmonic Synthesis with uncompensated topography.

EGM96 truncated at degree and order 180 and the Airy-compensated Δg field (equations (58) & (89)). Fig. 13 shows a worldmap and a histogram of the difference between EGM96 and the Airy-compensated gravity anomalies. Finally Fig. 14 displays the analogous computations applying the Pratt isostatic model (equations (84) – (87) & (89)). These images provide a first picture of the effect of compensation in the computation of topographic/isostatic potential harmonic coefficients. First of all one notices that the ‘observed’ gravity anomaly field given by the truncated EGM96 model hardly shows a correlation with the topography. This changes with the topographic/isostatic gravity fields. A separation between continental and ocean areas is noticeable with the Airy-compensated gravity anomalies; this pattern is much more obvious for the uncompensated and the Pratt global gravity anomaly fields. While with the Airy compensation the continental part is separated more clearly from the oceans than the EGM96 field, the compensation with the Pratt model removes the topographic signal in a much more evident manner as Fig. 14 indicates. However, both models seem to fail in

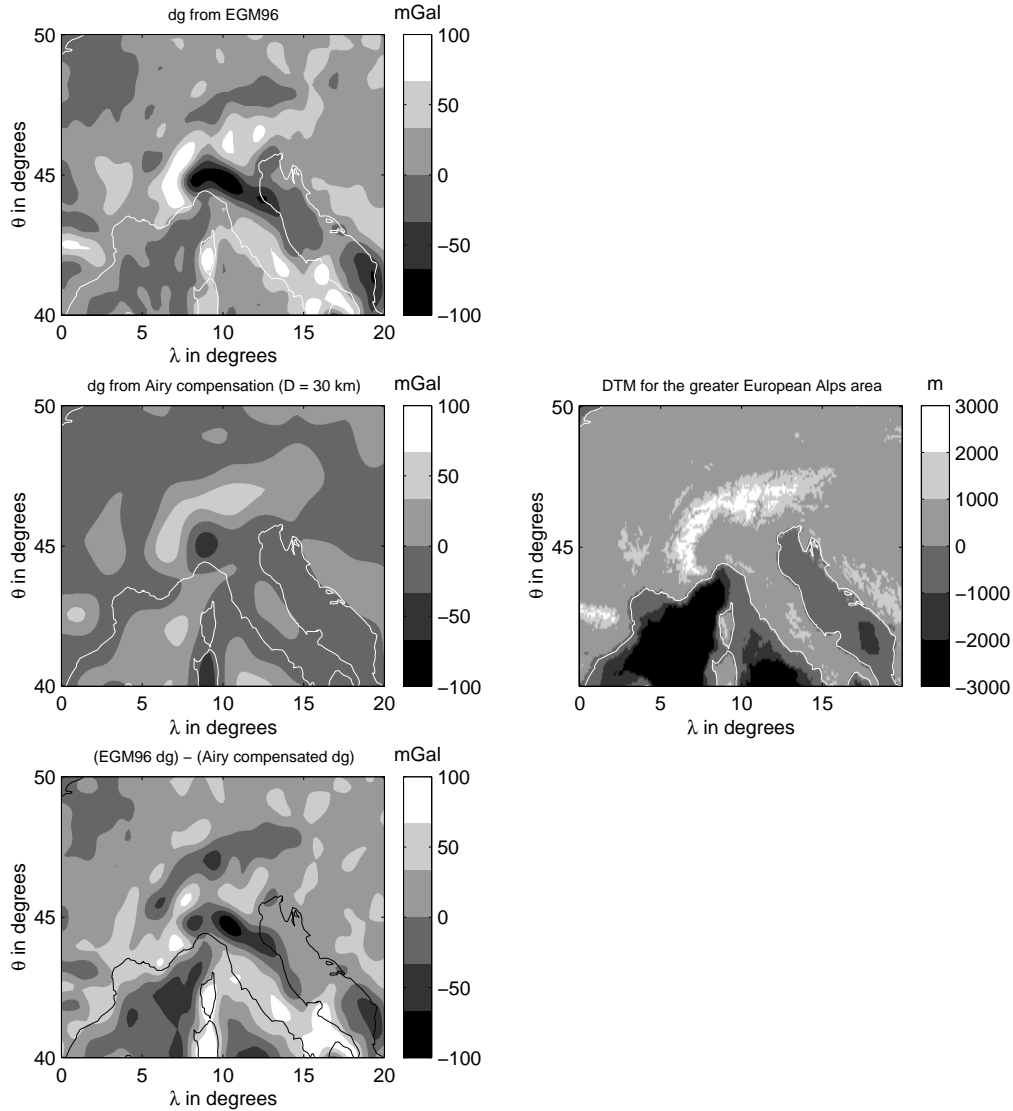


Figure 16: Regional Spherical Harmonic Synthesis with Airy-compensated topography.

meeting the requirements of a compensation in a global scale. As Figures 13 and 14 indicate the differences between both isostatic models and EGM96 are hardly smoother than EGM96 itself. Although in the case of the Airy compensation the differences to EGM96 are mainly concentrated in the range of $[-50, 50]$ mGal, in both models the differences reach values clearly greater than the maximum or minimum values of the EGM96 field as the histogram of the latter in Fig. 13 displays. Thus, both Airy and Pratt isostasy, since they represent an idealized situation and are perhaps more appropriate for applications in a local scale, they seem inappropriate when applied globally. On the one hand applying both models results in the removal of the topographic signal, with the Pratt model being the most evident example. However, none of the models succeeded in smoothing the EGM96 model. On the contrary, the topographic/isostatic coefficients due to their dependence on the terrain cannot be reasonably compared to the EGM96 coefficients nor are they appropriate e.g. for an evaluation of a global geoid.

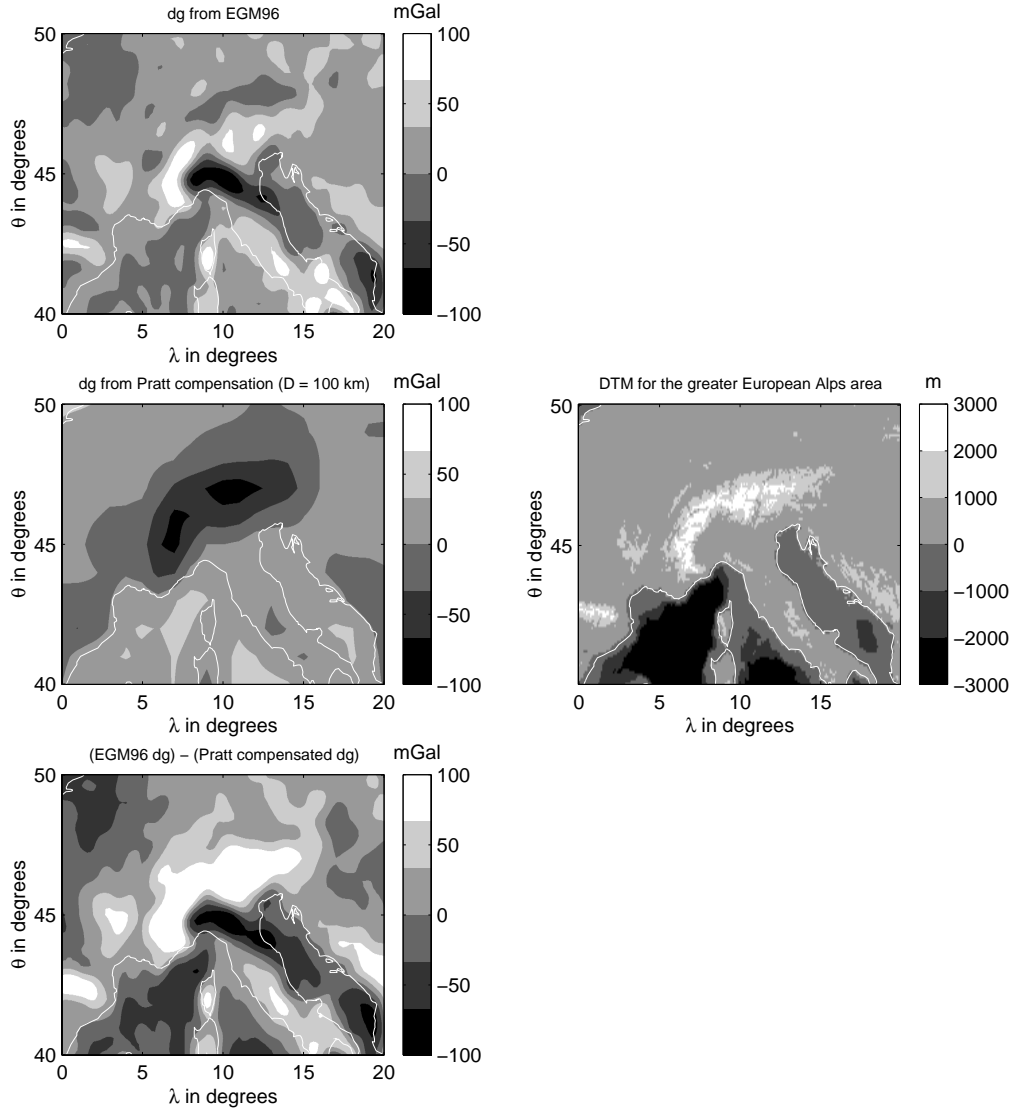


Figure 17: Regional Spherical Harmonic Synthesis with Pratt-compensated topography.

10 Regional Spherical Harmonic Synthesis applications

We conclude our numerical investigations by presenting some examples of spherical harmonic synthesis in a regional scale. The structure of the involved matrices given in section 2 permits such a computation. The only modification is to insert the θ and λ vectors, which correspond to the area in question in the respective matrices instead of $\theta_i = \Delta\theta/2 + i\Delta\theta$, $i = 0, 1, \dots, L-1$ and $\lambda_j = \Delta\lambda/2 + j\Delta\lambda$ with $j = 0, 1, \dots, 2L-1$, which represents an equi-angular global grid of point data centered at the cells built by the grid of meridians and parallels (block centers). The area surrounding the European Alps was selected for our computations and three different color maps were produced: Fig. 15, Fig. 16 & Fig. 17. These plots show gravity anomalies Δg as computed by uncompensated topography, by

the Airy and by the Pratt compensation models respectively. Also the local applications should not be overestimated. No one should expect to recognize local structures or make easier geophysical interpretations than the respective global plots. The reason is simple: for these ‘regional’ computations the same global \overline{C}_{lm} and \overline{S}_{lm} set is used, only the output matrix of Δg has been changed. Thus, figures 15 – 17 should be regarded as a magnification of the respective global plots where we zoom into the specific area. Apart from that, all the uncertainties or errors of the coefficients are propagated into these computations as well. In this sense, the picture we obtain from these regional applications in comparison to the global fields is more or less the same. The evaluation of a gravity anomaly field using topographic/isostatic coefficients makes the field more terrain dependent than the one computed from The EGM96 model. Compared to the observed field EGM96 however, both isostatic models clearly fail to improve the picture in a substantial way: the differences with EGM96 for Airy as well for Pratt approach the behaviour of EGM96 itself.

11 Conclusions

This report discusses two different issues in spherical harmonic analysis: global spherical harmonic analysis and synthesis with point and mean data and the computation of topographic/isostatic potential harmonic coefficients. Although these subjects can be investigated independently, they are dealt with here under the ‘generic’ term of global spherical harmonic computations. The loss of orthogonality of the Legendre functions in the transition from the continuous to the discrete case complicates spherical analysis and imposes the assignment of certain weights to the θ -samples. Employing block means instead of point values requires the use of the integrals of the associated Legendre functions. A recursion scheme similar to the one for the associated Legendre functions enables such a computation. The theory for the computation of topographic/isostatic potential harmonic coefficients was reviewed in detail. For this purpose the idealized isostatic models of Airy/Heiskanen and Pratt/Hayford were taken into consideration. Spherical harmonic synthesis applications in a global and regional scale were performed using the obtained set of topographic/isostatic coefficients. These computations indicate that both models seem to be inappropriate for large spatial scales, with the respective global fields being not comparable to the observed gravity field of EGM96. Furthermore, the topographic/isostatic gravity field exposes, as expected, terrain-dependent patterns. The obtained potential coefficients are therefore inappropriate for computations of functionals of the gravity field in a global as well as on a regional scale.

Acknowledgments

I would like to thank Prof. Dr.–Ing. R. Rummel for carefully reading the manuscript and for his constructive comments. The global spherical harmonic analysis package was developed in MATLAB v. 5.2 and includes m-file `gsha.m` for global spherical harmonic analysis for any of the five methods listed in section 2 or with employing mean values. The latter method (`mean`) uses `iplm.m` which evaluates the integrals of the associated Legendre functions. The m-file `iplmquad.m` and the function `intpnm.m` were also written to test the recursive computations done by `iplm.m`, by performing a numerical quadrature. Ir. Nico Sneeuw supervised the whole effort and had always time for discussions and useful MATLAB-suggestions. The applications in sections 9 and 10 were performed using following m-files developed by Sneeuw: `gshs.m`, `rshs.m` for global and regional spherical harmonic analysis respectively and `plm.m` for the recursive computation of the fully normalized associated Legendre functions. Last but not least, financial support through a scholarship by the German Academic Exchange Program (DAAD) is gratefully acknowledged.

References

- Albertella A. and F. Sacerdote (1995): Spectral analysis of block averaged data in geopotential global model determination, *Journal of Geodesy*, **70**, 166–175.
- Colombo O.L. (1981): Numerical methods for harmonic analysis on the sphere, *Department of Geodetic Science and Surveying*, Rep. No. 310, The Ohio State University, Columbus, Ohio.
- Gerstl M. (1980): On the recursive computation of the integrals of the associated Legendre functions, *manuscripta geodaetica*, **5**, 181–199.
- Heiskanen W.A. and H. Moritz (1967): *Physical Geodesy*, W.H. Freeman and Co., San Francisco.
- Hobson E.W. (1955): *The Theory of Spherical and Ellipsoidal Harmonics*, Cambridge University Press, U.K.
- Krylov V.I. (1962): *Approximate Calculation of Integrals*, MacMillan, New York.
- Lambeck K. (1988): *Geophysical geodesy. The slow deformations of the Earth*, Clarendon Press, Oxford.
- Lemoine F.G., S.C. Kenyon, J.K. Factor, R.G. Trimmer, N.K. Pavlis, D.S. Chinn, C.M. Cox, S.M. Klosko, S.B. Luthcke, M.H. Torrence, Y.M. Wang, R.G. Williamson, E.C. Pavlis, R.H. Rapp and T.R. Olson (1998): The Development of the Joint NASA GSFC and the National Imaginery and Mapping Agency (NIMA) Geopotential Model EGM96, NASA/TP-1998-206861, Goddard Space Flight Center, Greenbelt, Maryland.
- Lense J. (1954): *Kugelfunktionen*, Akademische Verlagsgesellschaft, Leipzig.
- Paul M.K. (1978): Recurrence relations for integrals of the associated Legendre functions, *Bulletin G eod esique*, **52**, 177–190.
- Rapp R.H. (1982): Degree variances of the Earth’s potential, topography and its isostatic compensation, *Bulletin G eod esique*, **56**, 84–94.
- Rummel R., R.H. Rapp, H. S unkel and C.C. Tscherning (1988): Comparisons of global topographic/isostatic models to the Earth’s observed gravity field, *Department of Geodetic Science and Surveying*, Rep. No. 388, The Ohio State University, Columbus, Ohio.
- Rummel R. (1991): *Physical Geodesy, Parts I & II*, Lecture Notes, Technical University of Delft, Department of geodesy.
- Rummel R. and M. van Gelderen (1995): Meissl scheme – spectral characteristics of physical geodesy, *manuscripta geodaetica*, **20**, 379–385.
- Sneeuw N. (1994): Global spherical harmonic analysis by least-squares and numerical quadrature methods in historical perspective, *Geophysical Journal International*, **118**, 707–716.
- Strang G. (1986): *Introduction to Applied Mathematics*, Wellesley–Cambridge Press, Cambridge, MA.
- S unkel H. (1986): Global topographic-isostatic models, In: *Mathematical and Numerical Techniques in Physical Geodesy*, H. S unkel (Editor), 417–462, Lecture Notes in Earth Sciences, Springer-Verlag, Berlin.
- Wieser M. (1987): The Global Digital Terrain Model TUG87, internal report, Technical University of Graz, Institute of Mathematical Geodesy.